AD-A095 147 WYOMING UNIV LARAMIE DEPT OF MECHANICAL ENGINEERING F/G 11/4
THREE-DIMENSIONAL ELASTOPLASTIC FINITE ELEMENT ANALYSIS OF LAMI--ETC(U)
NOV 80 M M MONIB, D F ADAMS, D E WALRATH DAAG29-79-C-0189
UNCLASSIFIED UWME-DR-001-102-1 ARO-16370.4-MS NL

1 OF 2
AD A095 147

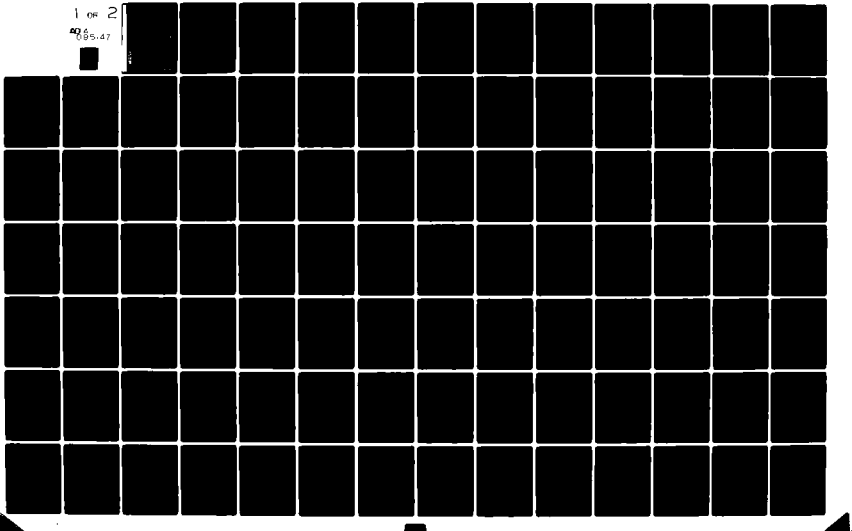

DEPARTMENTAL REPORT UWME-DR-001-102-1

THREE-DIMENSIONAL ELASTOPLASTIC FINITE ELEMENT ANALYSIS OF LAMINATED COMPOSITES

12

LEVEL II

Mohamed M. Monib
Donald F. Adams

November 1980

INTERIM REPORT
U.S. Army Research Office
Grant No. DAAG 29-79-C-0189

COMPOSITE MATERIALS RESEARCH GROUP
DEPARTMENT of MECHANICAL ENGINEERING
University of Wyoming Laramie, Wyoming 82071

THE VIEWS, OPINIONS, AND/OR FINDINGS CONTAINED IN THIS REPORT ARE THOSE OF THE AUTHORS AND SHOULD NOT BE CONSTRUED AS AN OFFICIAL DEPARTMENT OF THE ARMY POSITION, POLICY, OR DECISION, UNLESS SO DESIGNATED BY OTHER DOCUMENTATION.

(18) ARO

(19) 16370.4-ME

(14) DEPARTMENT REPORT
UWME-DR-001-102-1

(6)

THREE-DIMENSIONAL ELASTOPLASTIC FINITE ELEMENT ANALYSIS OF LAMINATED COMPOSITES

(9) INTERIM REPORT,

(16) MOHAMED M. MONIB
DONALD F. ADAMS
David E. Walrath

(11) NOVEMBER 1980

(12) 125

U.S. ARMY RESEARCH OFFICE
GRANT NO. (15) DAAG 29-79-C-0189

COMPOSITE MATERIALS RESEARCH GROUP
MECHANICAL ENGINEERING DEPARTMENT
UNIVERSITY OF WYOMING
LARAMIE, WYOMING 82071

408984

Unclassified

SECURITY CLASSIFICATION OF THIS PAGE (When Data Entered)

REPORT DOCUMENTATION PAGE	READ INSTRUCTIONS BEFORE COMPLETING FORM
1. REPORT NUMBER	2. GOVT ACCESSION NO. AD-A095 147 / 3. RECIPIENT'S CATALOG NUMBER
4. TITLE (and Subtitle) Three-Dimensional Elastoplastic Finite Element Analysis of Laminated Plates	5. TYPE OF REPORT & PERIOD COVERED Interim Report
	6. PERFORMING ORG. REPORT NUMBER UWME-DR-001-102-1
7. AUTHOR(s) Mohamed M. Monib, Donald F. Adams	8. CONTRACT OR GRANT NUMBER(s) DAAG 29-79-C-0189
9. PERFORMING ORGANIZATION NAME AND ADDRESS Composite Materials Research Group, Mechanical Engineering Department, University of Wyoming, Laramie, Wyoming 82071	10. PROGRAM ELEMENT PROJECT, TASK AREA & WORK UNIT NUMBERS
11. CONTROLLING OFFICE NAME AND ADDRESS U.S. Army Research Office, P.O. Box 12211, Research Triangle Park, N.C. 27709	12. REPORT DATE November 1980
	13. NUMBER OF PAGES 111
14. MONITORING AGENCY NAME & ADDRESS(if different from Controlling Office)	15. SECURITY CLASS. (of this report) Unclassified
	15a. DECLASSIFICATION/DOWNGRADING SCHEDULE N.A.

16. DISTRIBUTION STATEMENT (of this Report)

Approved for public release; distribution unlimited.

17. DISTRIBUTION STATEMENT (of the abstract entered in Block 20, if different from Report)

N.A.

18. SUPPLEMENTARY NOTES

The view, opinions, and/or findings contained in this report are those of the authors and should not be construed as an official Department of the Army position, policy, or decision, unless so designated by other documentation.

19. KEY WORDS (Continue on reverse side if necessary and identify by block number)

Composite Materials	Finite Element Analyses
Elastoplasticity	Laminate Analyses
Orthotropic Laminates	Thermal Effects
Interlaminar Stresses	Moisture Effects

20. ABSTRACT (Continue on reverse side if necessary and identify by block number)

A three-dimensional elastoplastic analysis of generally orthotropic composite laminates is developed, together with a finite element computer code NCLAP (nonlinear Composite Laminate Analysis Program) for its implementation. The analysis is capable of handling any laminated composite subjected to triaxial mechanical and/or hygrothermal loading conditions. The laminates can consist of any number of orthotropic material plies, of any orientations. Elastoplastic material behavior is included by means of the tangent modulus method. The onset of plastic deformation is determined by a failure surface in

DD FORM 1 JAN 73 1473 EDITION OF 1 NOV 65 IS OBSOLETE

Unclassified

SECURITY CLASSIFICATION OF THIS PAGE (When Data Entered)

three-dimensional space, and is likewise dependent on temperature and moisture.

The three-dimensional finite element analysis is based on a displacement formulation employing linear isoparametric elements. Large aspect ratios, typical of laminae finite element representations, are handled by the use of reduced integration techniques. Material properties are input to NCLAP as coefficients of second order polynomials describing the elastoplastic response, and the dependence on temperature and moisture content. Incremental mechanical loadings can be applied as nodal forces and/or prescribed displacements. Hygrothermal loadings are applied as constant overall changes, or as spatial distributions, of temperature and moisture content. Computer Program NCLAP has been developed in modular form, which will permit it to be easily modified to accommodate future extensions of the analysis.

FORWARD

This Interim Report presents the preliminary results of one phase of a comprehensive study, "Laminate Analyses, Micromechanical Creep Response, and Fatigue Behavior of Polymer Matrix Composites," being performed under Grant DAAG 29-79-C-0189 for the U.S. Army Research Office, Durham, North Carolina. The grant was initiated in September 1979. The ARO Program Monitor is Dr. John C. Hurt, Associate Director Metallurgy and Materials Science Division.

Program Manager and Principal Investigator at the University of Wyoming is Dr. Donald F. Adams, Professor of Mechanical Engineering. Co-Principal Investigator is Mr. David E. Walrath, Staff Scientist in Mechanical Engineering.

The task being reported here was performed by Dr. Mohamed M. Monib, as a Ph.D. Dissertation under the direction of Dr. D.F. Adams. Dr. Monib's work was initiated in late 1978 as an in-house project, and completed under the present grant.

The authors wish to thank the staff of the Mechanical Engineering Department for their contributions, and Dr. A. Keith Miller, Sandia Laboratories, Albuquerque, New Mexico, a former colleague at the University of Wyoming, for his many helpful discussions.

TABLE OF CONTENTS

LIST OF FIGURES

FIGURE PAGE

LIST OF TABLES

LIST OF SYMBOLS

$[B]$	Element shape matrix
$\bar{C}_{ij}$	Stiffness coefficients in the generally orthotropic stiffness matrix
$[C^e]$	Elastic stiffness matrix
$[C^P]$	Plastic stiffness matrix
$\{d\}$	Nodal displacement vector
$\bar{E}$	Initial slope of the effective stress effective strain curve
$\bar{E}_T$	Tangent modulus of the effective stress effective strain curve
H'	Tangent modulus of the effective stress effective plastic strain curve
h	Hardening parameter
$[J]$	Jacobian matrix
$[k]$	Element stiffness matrix
ΔM	Moisture change
N_i	Shape functions
N_{ij}	Parameters of anisotropy
$[S^e]$	Elastic compliance matrix
ΔT	Temperature change
u,r,w	Node point displacements
α_i,α_j	Kinematic hardening parameters
$\alpha_1,\alpha_2,\alpha_3$	Coefficients of thermal expansion in the principal coordinate system
β_1,β_2,β_3	Coefficients of moisture expansion in the principal coordinate system

γ^e_{ij}	Elastic shear strain components
γ^p_{ij}	Plastic shear strain components
ε^e_{ij}	Elastic strain components
ε^p_{ij}	Plastic strain components
ε_o	Initial strains
$\bar{\varepsilon}$	Effective strain
ν_{ij}	Poisson's ratios
$\bar{\sigma}$	Effective stress
σ_{ij}	Stress tensor
$d\lambda$	Lagrange multiplier
τ_{ij}	Shear stress components

SECTION 1

INTRODUCTION

Much has been heard about the advantages of advanced composite materials which accrue because of their high specific stiffness and strength, excellent damage tolerance, and superior fatigue response characteristics, as well as their corrosion resistance in hostile environments. Laminated composites are in increasing demand, because they can actually be tailored by the design engineer to suit almost any particular application. These laminates are fabricated by stacking up plies or laminae of unidirectional fibrous composites, with each lamina oriented in different directions to achieve the required stiffness and strength.

With the increased use of laminated composites, analytical tools are needed for the prediction of the laminate behavior. The so-called classical laminated plate theory has long been used by many designers to predict laminate response. Occasionally, others have used finite difference or two-dimensional finite element methods to predict the laminate response. These methods, however, are limited in their capabilities. The classical laminated plate theory, for example, neglects certain stress components which experimental observations have shown to play an important role in failure of laminated composites. Experimental observations have also shown that many laminated composites exhibit significant amounts of inelastic

behavior, and that yielding of a ply or lamina within a laminate does not mean failure of the laminate. Approximate methods typically neglect this inelastic behavior. Furthermore, the effect of changes in temperature and moisture on the material properties is usually neglected in these analyses.

In the present work, the full three-dimensional problem of laminated composites has been addressed. A plasticity model that takes into account the effect of varying material properties due to temperature and moisture changes has been developed to describe the inelastic behavior of the laminate in three-dimensional space. This model has been developed in such a way as to make it possible to incorporate it in a three-dimensional finite element analysis. A computer program has been developed for the implementation of the analysis. Both mechanical and hygrothermal loading conditions can be handled by this three-dimensional elastoplastic finite element program.

In Section 2, an historical background of the analysis of composite laminates is presented. The classical theory of laminated plates and other analytical methods are reviewed. Linear and nonlinear approximate analyses cited in the literature are also discussed and studies of thermal stresses and interlaminar stresses are presented.

In Section 3, the concepts of yield criterion, hardening rule, and flow rule are examined in view of previous studies in the literature. A plasticity model that accounts for varying temperature

and moisture content, and leads to a stiffness concept suitable for use in a three-dimensional finite element analysis, is then developed. Finally, the finite element analysis and the main features of the associated computer code, developed as the tool for this work, are discussed. Example problems are presented with results and discussion in Section 4, and a general discussion, summary, and suggestions for future work are included in Section 5.

SECTION 2

LITERATURE REVIEW

2.1 Linear Analyses

Tsai [1] was among the first investigators to apply the classical laminated plate theory to composite materials. The classical laminated plate theory (LPT) that he presented in 1964 is based on the work by Reissner and Stavsky [2] in 1961. Even earlier works, such as that of Smith [3] published in 1953, should also be considered to have contributed to the development of the laminated plate theory. Smith assumed plane stress conditions in his work on orthotropic plywood. A detailed description of the laminated plate theory is given in Reference [4]. The work by Tsai [1] is a point stress analysis in that it does not take into account boundary conditions. Ashton and Whitney [5] applied LPT to the problem of laminated plates and presented solutions that satisfied the boundary conditions for specially orthotropic plates, i.e., laminated plates composed of orthotropic layers such that the orthotropic axes of symmetry of each layer coincide with the geometric axes of the plate. This type of laminate does not exhibit coupling between the bending moment resultants and the twisting curvatures.

Although thermal loading is handled by the laminated plate theory, to date few attempts [6] have been made to consider varying material properties due to temperature, and none for humidity changes. Also a significant limitation of LPT is that it cannot

consider the out-of-plane stresses which, as will be seen later in this chapter, have proven to be of great importance in the analysis of composite materials. Some computer codes based on LPT are still widely used, e.g., AC3 [7] and SQ5 [8].

Tsai [1] developed an analytical method to predict the elastic constants of a lamina based upon the properties of the fibers and the matrix material. Then, using the laminated plate theory, he theoretically predicted the elastic constants of laminates made of glass/epoxy plies. With the aid of an experimental technique, Azzi and Tsai [9] were able to show good agreement between the analytical predictions and experimental results for glass/epoxy composites. Hill's yield condition [10] for orthotropic materials under plane stress conditions was employed to predict laminate failure in an analytical study [11] of the strength of transversely isotropic laminates. Inelastic behavior was not included in this study, however.

In 1965, Tsai [12] considered both mechanical and thermal loading in his method for modeling the load transfer from one lamina as it failed to the remaining unfailed laminae. Lamina failure was predcited using Hill's plane stress yield condition [10]. After the failure of a lamina, the stiffness matrix was degraded by setting the appropriate elastic constants to a small fraction of their original values. However, all laminae were assumed to remain *linearly elastic to failure.*

The concept of a stepwise reduction in load carrying capacity after a lamina reached initial yielding according to Hill's yield

condition was used by Chiu [13]. He noted that failure in one direction of a certain lamina did not imply total failure of this particular lamina, or failure of the laminate. Out-of-plane stresses were not included in this study, however, and no account was made for hygrothermal effects.

In 1967, Hoffman [14] proposed a failure criterion similar to Hill's [10] yield condition. His theory contained linear terms and hence could account for differing tensile and compressive properties. Good agreement between theory and experiment for the ultimate strength of laminates was shown for uniaxial tensile and compressive tests; no account was made of the initial thermal stresses which are induced during the fabrication of composite materials, due to the cooldown from high curing temperatures.

In 1971, Tsai and Wu [15] proposed a general strength criterion for anisotropic materials. They employed an analytical method that assumed the stress-strain curve to be elastic to failure. Limited uniaxial experiments showed good agreement with theoretical predictions for ultimate strength of graphite/epoxy. This strength theory and others will be discussed in more detail when yield surfaces are considered in the next chapter.

During the fabrication of composite laminates, residual thermal stresses are induced due to cooldown from the cure temperature. The important effect of these thermally-induced stresses has long been recognized in studies of unidirectional composites, by investigators such as Adams and Doner [16], Foye [17], and Miller and Adams [18,19].

However, in spite of this activity, in 1974 Hahn and Pagano [6] noted that no method was yet available that would account for these stresses in composite laminates. They developed a method based on total stress-strain-temperature relations. Strains were assumed to consist of thermal strains and mechanical strains, with the latter depending also on temperature. Material stiffnesses were assumed to depend only linearly on temperature. By employing the laminated plate theory, however, they carried along all its limitations explained earlier. Their method did not consider nonlinear material effects.

2.2 Nonlinear Analyses

Throughout this work, the terms nonlinear elastic, inelastic, and elastoplastic will be used to describe material response. Nonlinear or nonlinear elastic behavior implies that unloading from any state of stress is assumed to follow the stress-strain curve, i.e., no permanent deformation occurs. Inelastic is used to describe the material behavior beyond its elastic limit. The term elastoplastic is used to describe materials which exhibit plastic (time-independent) deformations beyond the elastic limit.

With the development of high modulus fibers in the early 1960's, and hence the so-called advanced composites, the use of composites increased sharply. To be able to fully utilize these new materials, a full and complete understanding of their behavior was needed. Among many other needs, this increased the demand for nonlinear analyses.

An early attempt was that of Petit and Waddoups [20] in 1969. The laminate behavior was established by a piecewise linear approach, and incremental application of average laminate stresses. At each increment of load, the incremental strains were determined and added to previous strains to determine the total strains in each lamina. These were then transformed to the principal directions of the lamina. Lamina principal strains were then referred back to the respective stress-strain curves, which were composed of linear segments, and updated stiffnesses were determined for the next load increment. Failure was assumed to occur when a principal strain reached a corresponding ultimate value in any lamina. Inelastic material behavior was not considered, however. No accounting of thermal effects was made, and being a two-dimensional analysis, the important role of out-of-plane stresses on failure mode could not be handled. In a similar analysis by Hashin, et. al. [21], the Ramberg-Osgood equation [22] was used to represent the lamina stress-strain curves, this being a three-parameter curve-fit equation.

Cubic spline interpolation curve-fit functions were employed by Sandhu [23] to model the lamina stress-strain curves. Incremental loading was used, the material properties being updated each increment using equivalent strains. Sandhu proposed that it was erroneous to determine updated material properties after each loading increment based on the individual lamina strains, as in the work of Petit and Waddoups [20]. He assumed that the incremental stresses could be related to the incremental strains. The ultimate load carrying

capacity of the laminate was determined by the plywise application of a failure criterion which assumed that the strain energies under longitudinal, transverse and shear loadings were independent parameters. Better agreement between theory and experiment for various boron/epoxy laminates than that reported by Petit and Waddoups [20] was also indicated. Sandhu did not consider hygrothermal loading in his analysis, and no yield criterion was used, i.e., inelastic effects were neglected.

Nonlinear behavior of laminated fibrous composites including thermal effects and temperature-dependent material properties was considered in a study by Renieri and Herakovich [24]. Using a two-dimensional finite element analysis and limiting the loading conditions to uniaxial mechanical loading, they studied both nonlinear and thermal effects. They showed that these effects are important in the prediction of failure modes in composite laminates, and noted that laminate failure is a function of the laminate configuration, material, and type of loading. Unloading was assumed to follow the stress-strain curve. No yield criterion was used in this two-dimensional analysis, i.e., inelastic behavior was neglected, and failure was assumed when any of the strains in the principal directions of the material reached its ultimate value. The analysis was also restricted to symmetric laminates.

2.3 Interlaminar Stresses

A characteristic of laminated composites is that under in-plane uniaxial or biaxial loading conditions, a laminate often develops

triaxial effects, i.e., a laminate under in-plane loading only will often, depending on its lay-up, develop out-of-plane stresses. These out-of-plane stresses are termed interlaminar stresses. Their effect is most significant near free edges where they attain high values.

Plane stress conditions assumed in the classical laminated plate theory do not allow for the calculation of interlaminar stresses. Rather, only the stresses in the plane of the laminate are considered. The laminated plate theory is thus incapable of providing predictions of some of the stresses that actually cause failure of composite laminates, as shown by experimental evidence [25]. In fact, interlaminar stresses are one of the mechanisms that uniquely characterize failure in composite laminates. These stresses may cause delamination near a free edge, whether it be at the edge of a plate, around a hole, etc. Their effect near an edge is known as the free edge effect.

In an effort to evaluate interlaminar stresses and the influence of the stacking sequence on laminate strength under uniform axial loading, Pipes and Pagano [26] used a finite difference technique. Their study was limited to angle-ply laminates, i.e., laminates with an even number of layers, with each lamina or ply alternately oriented at $+\theta$ and $-\theta$ to one of the geometric axes in the plane of the laminate. They noted that significant interlaminar shear stresses were required to allow shear transfer between the plies of the laminate. In addition, the interlaminar normal stress was found to be an

edge effect, restricted to a region near the free edge approximately equal to the laminate thickness. They reported strong evidence of a singularity in interlaminar normal stress at the intersection of an interface and the free edge. They also suggested that such high stresses in the neighborhood of the free edge may be expected to cause delamination of the laminate, in particular under fatigue loadings. Experimental observations of this phenomenon had been reported earlier by Foye and Baker [27]. Similar results were also reported by Pipes and Daniel [28], in their work on graphite/epoxy. Interlaminar stress results for cross-ply graphite/epoxy laminates, i.e., laminates with alternating 0° and 90° plies, and other laminate configurations, subjected to uniform axial strain loading are reported in Reference [29].

Finite difference and finite element methods [30-42] both have been used to determine the interlaminar stresses due to in-plane loading of laminates. Relatively little work has been done to determine these stresses due to hygrothermal loading or nonlinear effects, in spite of their importance.

Among the first to use a finite element analysis to determine interlaminar stresses were Puppo and Evensen [30], and Isakson and Levy [31]. Those investigators assumed plane stress conditions, and the fibrous laminae were considered to be orthotropic layers separated by isotropic laminae of finite thickness that developed only interlaminar shear stresses. Due to the assumed plane stress conditions, however, interlaminar normal stresses could not be

modeled. This work and that of Reference [30] assumed linearly elastic material behavior. Levy, et. al. [32], extended the work of Isakson and Levy [31] to include plastic deformation of the shear layer, but due to the use of two-dimensional analysis and the assumed plane stress conditions, they were again unable to handle the interlaminar normal stresses. These studies were also limited to mechanical loadings.

Herakovich and Brooks [33] considered laminates in the elastic range under uniform axial strain loading. They used a finite element analysis [27], and finite element subsections at the free edge were considered, i.e., the finite element solution was reapplied to smaller sections near the free edge to obtain more detail in this region. Relatively high interlaminar stresses at the free edge and at the lamina interface were predicted. They also pointed out the significance of the interlaminar stresses with respect to the applied loads and the stacking sequence, and noted that the magnitude of the interlaminar stresses could influence the strength of the laminate. Again this analysis neglected nonlinear effects. To account for the interlaminar normal stresses, a linearly elastic three-dimensional finite element analysis was used by Rybicki [34]. He was able to consider both interlaminar shear and normal stresses. The effects of stacking sequence were studied under mechanical loading only.

Very recently, Altus, et. al. [35], presented a three-dimensional finite difference solution of the problem of free edge effects. Only symmetric angle-ply laminates were considered in this linearly

elastic analysis. The finite difference grid consisted of real points inside the layer and fictitious points outside it to satisfy the boundary conditions on the faces of each layer. This study confirmed qualitatively that the normal interlaminar stresses represent one of the most significant factors affecting failure of laminates, a result which was also noted in previous studies [36-40]. These studies considered mechanical loadings only. Results for edge effects under mechanical as well as thermal loadings were reported by Wang and Crossman [41,42]. The material properties were assumed not to vary with temperature in their study, however.

Rybicki and Schmueser [43] studied the effect of stacking sequence and lay-up angle on free edge stresses around a hole in a laminated plate under tension. A three-dimensional analysis was used to determine the tangential strain distributions around circular holes in composite laminates under uniaxial loading. Interlaminar normal stress distributions around the free edge of the circular hole, changes in stacking sequence, and lay-up angle were also studied for different graphite/epoxy systems. They did not consider nonlinear or inelastic material behavior, however.

In summary, although nonlinear effects in advanced composite laminate systems, and both normal and shear interlaminar stresses, have been recognized to be of major importance in the prediction of laminate response to mechanical and hygrothermal loading conditions, to date no rigorous, fully three-dimensional nonlinear analysis has been developed. The aim of the present work is to do so.

SECTION 3

DEVELOPMENT OF ANALYSIS

Implicit in the development of any plasticity model are assumptions associated with the behavior of the material. Several of these assumptions will be employed in the present work; a discussion of their implications follows.

3.1 Yield Criterion

The initial yield condition defining the elastic limit of the material in a multiaxial stress state is referred to as the yield surface or the yield criterion. A discussion of the concept of yield surface is given in Reference [44].

The basic limitation of all present yield criteria is the lack of sufficient experimental data to support the mathematical model by which the yield surface is described. Phenomenological effects such as hardening, strain history dependence, and the Bauschinger effect [10] are difficult to determine, and vary among different materials. The Bauschinger effect accounts for having a different yield stress in compression than in tension after reversing the stress vector from any tensile plastic stress state, and vice versa, as seen in Figure 1. Since the exact role the Bauschinger effect plays in the behavior of composite materials is still unknown, this effect is often neglected in dealing with problems in plasticity. It will be neglected in the present analysis also.

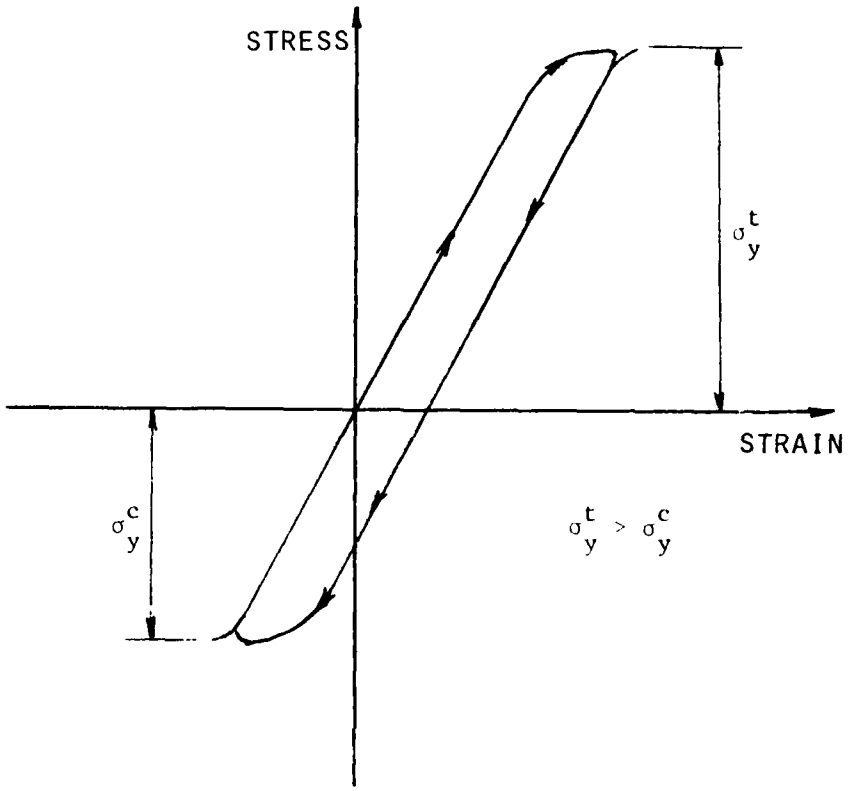

Figure 1. Bauschinger Effect

Among the most frequently used yield criteria are those attributed to Tresca [45] and von Mises [46]. The Tresca condition states that inelastic action at any point in a body begins only when the maximum shearing stress on some plane through the point reaches a value equal to the maximum shearing stress in a uniaxial tension specimen at yield. The more popular von Mises criterion [46] has been extended to describe anisotropic materials [10,47-50]. In the work by Yamada [48], the yield condition was assumed to be quadratic in the stress components, and to reduce to the von Mises criterion when

the degree of anisotropy was small. The Hill yield criterion [10] took the form

$$f(\sigma_k) = N_{ij}\sigma_i\sigma_j - 1 = 0 \qquad (1)$$

where N_{ij} are constants related to the six yield stresses in the principal anisotropic directions.

Implicit in Hill's criterion are:

1) The principal axes of anisotropy do not rotate during plastic flow.
2) Orthotropic material behavior is assumed.
3) The principal axes of anisotropy either coincide with the principal stress axes or the transformation is known.
4) The anisotropic parameters N_{ij} remain unchanged during plastic flow.

Baltov and Sawczuk [51] generalized Hill's yield criterion to include combined isotropic and kinematic hardening. (Both will be presented in a later section). They assumed a form

$$f(\sigma_k) = N_{ij}(\sigma_i - \alpha_i)(\sigma_j - \alpha_j) - 1 = 0 \qquad (2)$$

where α_i and α_j are the kinematic hardening parameters. The anisotropic parameters N_{ij} are prescribed functions of the plastic strain, and hence change during the course of plastic flow.

Several investigations have been concerned with defining a strength criterion specifically for composite materials. A criterion of this type is used as a failure surface or condition in stress

space. When the stress state, expressed as some function of the stress components, lies on this surface, it satisfies the failure condition. That is, the material is assumed to have failed. These surfaces could also be used to define yielding, if the parameters describing such surfaces were expressed in terms of material yield stresses instead of material ultimate strengths.

One criterion of the type described above is the Tsai-Hill criterion [52]. In fact, this strength criterion is based on Hill's yield criterion [10]. Tsai related the anisotropic parameters to the usual failure strengths σ_1^u, σ_2^u, and τ_{12}^u of a lamina. For plane stress conditions, it takes the form

$$\frac{\sigma_1^2}{(\sigma_1^u)^2} + \frac{\sigma_2^2}{(\sigma_2^u)^2} - \frac{\sigma_1\sigma_2}{(\sigma_1^u)^2} + \frac{\tau_{12}^2}{(\tau_{12}^u)^2} = 1 \qquad (3)$$

Considerable interaction exists between the failure strengths σ_1^u, σ_2^u, and τ_{12}^u of this theory and those of other criteria which assume that axial, transverse, and shear failures occur independently. A typical element of a fibrous composite lamina is shown in Figure 2. The three principal axes are: 1 in the direction of the fibers, 2 transversely in the plane, and 3 normal to the plane of the lamina.

Another strength criterion was presented by Tsai and Wu [15]. Their assumption was

$$f(\sigma_k) = N_i\sigma_i + N_{ij}\sigma_i\sigma_j = 1 \qquad (4)$$

where N_i, N_{ij} are strength tensors of the second and fourth order, and are functions of independent material strengths. The linear term in this form can be used to account for the difference between tensile and compressive properties. Several features of this strength criterion are:

1) It is a scalar equation and is invariant, i.e., interactions between the stress components are independent material properties.
2) Since the strength components are expressed as tensor polynomials, their transformation relations and the associated invariants are well established.
3) Material axes can be rotated from N_i to N_i' and N_{ij} to N_{ij}' in Eq. (4), provided the transformation relations are known.

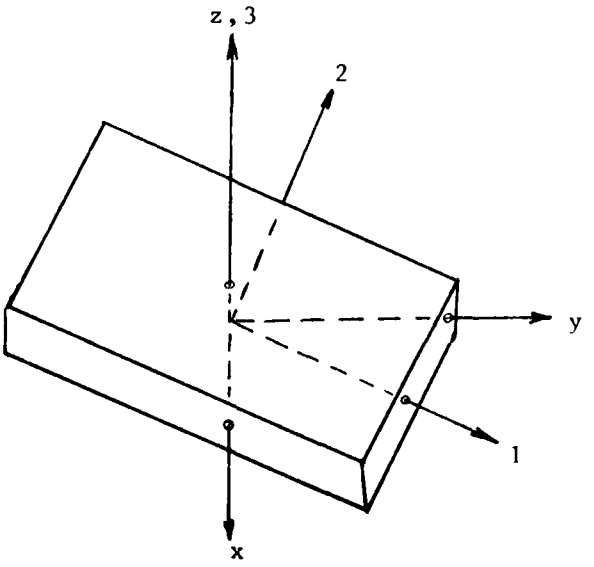

Figure 2. Unidirectional Fibrous Lamina

Although it seems physically attractive, some components in the tensor polynomial require difficult and expensive biaxial testing for their determination. Narayanaswami and Adelman [53] proposed a modified criterion, based on the Tsai-Wu theory, in which terms requiring biaxial testing were assumed zero. This criterion could also be modified and used as a yield criterion.

3.2 Hardening Rule

The stress-strain response after initial yielding differs among various materials, and it also differs among various plasticity theories. This post yielding response, called hardening, is described by specifying a subsequent yield surface, often termed the loading surface or the hardening rule. An account of the various hardening rules currently used is given by Armen [54].

The choice of a hardening rule will depend on its ability to represent the hardening behavior of the material under consideration, and upon the ease with which it can be applied. These requirements, together with the necessity of maintaining mathematical consistency with the yield function described in the previous section, constitute the criterion for the selection of a hardening rule.

Hill [10] and Hodge [55] proposed the isotropic hardening rule, which assumed that during plastic flow the loading surface expanded uniformly about the origin in stress space, maintaining the same shape, center and orientation as the yield surface. Figure 3 illustrates the yield and loading surfaces when the stress state shifts from point 1 to point 2. Unloading and subsequent reloading

in the reverse direction will result in yielding at the stress state represented by point 3. The path 2-3 will be elastic, and 0-2 is equal to 0-3. The isotropic representation of work hardening does not account for the Bauschinger effect. Since fibrous composites are strongly anisotropic, the directions of anisotropy remain effectively unchanged during deformation. Thus, the isotropic work hardening rule is suitable for these materials.

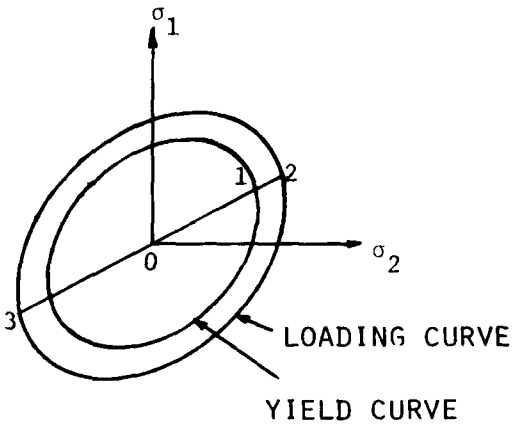

Figure 3. Isotropic Hardening

The hardening behavior postulated in the theory of kinematic hardening is due to Prager [56,57], and assumes that during plastic deformation the loading surface translates in stress space, maintaining the size, shape, and orientation of the yield surface. The primary aim of this theory is to provide a means of accounting for the Bauschinger effect. Figure 4 is an illustration of kinematic hardening. The yield surface and loading surface are shown in this

figure for a shift of the stress state from point 1 to point 2. The translation of the center of the yield surface is denoted by α_{ij}.

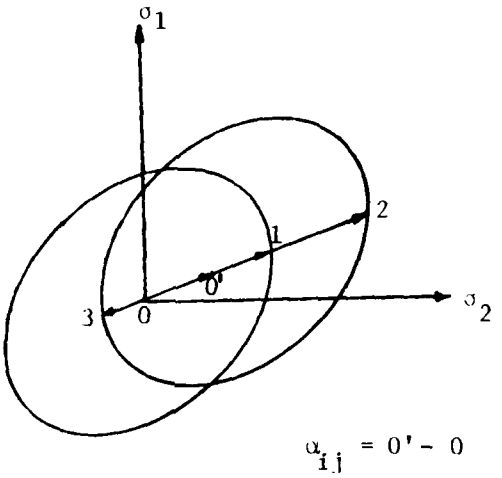

Figure 4. Kinematic Hardening

A model of combined kinematic and isotropic hardening, in which the subsequent loading surfaces expand and translate, has been presented by Hodge [58]. However, since there are no published experimental data that show that this model fits the behavior of composites, its complexity does not justify its use. Other hardening rules, proposed initially for metals, are discussed in References [59-63]. To date, there is no universally applicable model to describe all aspects of nonlinear material behavior. There are, however, some models better suited to specific needs than others. For a particular class of problems, the preferred model is that which best combines mathematical and computational simplicity with a proper

representation of experimentally observed behavior.

3.3 Flow Rule

Plastic strain increments are related to their corresponding stress increments by means of a flow rule. A general approach for determining a flow rule is the use of the concept of a plastic potential. The assumption is made that there exists a scalar function of stress $f(\sigma_{ij})$, from which the components of plastic strain increment are proportional to $\frac{\partial f}{\partial \sigma_{ij}}$. If $f(\sigma_{ij})$ represents the yield surface in stress space, then the above assumption represents a result of Drucker's postulate [64], which states that the work done by an external agency during a complete cycle of loading and unloading must be non-negative. Furthermore, this assumption leads to an incremental or associated linear flow theory of plasticity, in which the increment of plastic strain is in the direction of the outward normal to the surface represented by $f(\sigma_{ij})$ in stress space, at the current value of stress. A strain rate vector deviating from the outward normal to the yield surface in a direction independent of the stress rate vector constitutes the nonassociated linear flow theories of plasticity. The nonassociated flow theories are particularly suitable for work-softening materials [65], and can reasonably fit the behavior observed in some soils.

An associated flow rule that is generally used to describe elastic-plastic behavior is the Prandtl-Reuss relation, which is a generalization of the Levy-Mises equations. The Prandtl-Reuss

assumption is that the plastic strain increments, $d\varepsilon_{ij}^{p}$, are proportional to the corresponding stress deviator, σ_{ij}', where the instantaneous non-negative value of the constant of proportionality is dependent on the work hardening. The concept of an effective stress and effective plastic strain [66] is in itself an assumption that is usually introduced to reduce the complexity of a multiaxial situation to one that can be related to uniaxial behavior. Thus, the proportionality parameter can be the ratio of the effective stress to the effective plastic strain increment.

3.4 Stiffness Concept

The three-dimensional problem of laminates of fibrous composites will be formulated and analyzed. The stiffness concept that leads to the finite element analysis will then be discussed in relation to the solution of elastoplastic problems in three-dimensional space.

A transversely isotropic unidirectional composite lamina will be assumed. If the three principal axes of anisotropy are taken to be; 1 in the direction of the fibers, 2 transversely in the plane, and 3 normal to the plane of the lamina, as shown in Figure 2, the 2-3 plane will be the plane of transverse isotropy. As discussed earlier, the directions of anisotropy will not change during deformation. A quadratic form in the six components of stress, similar to Hill's yield condition [10], can then be chosen in the form

$$2f(\sigma_{ij}) = F(\sigma_2 - \sigma_3)^2 + G(\sigma_3 - \sigma_1)^2 + H(\sigma_1 - \sigma_2)^2 + 2L\,\tau_{23}^2 + 2M\,\tau_{31}^2 + 2N\,\tau_{12}^2 = 1 \tag{5}$$

where F, G, H, L, M, and N are parameters characteristic of the current state of anisotropy.

In the present study, the parameters of anisotropy are allowed to vary with changes in temperature and/or moisture content. It can easily be shown [10] that

$$\frac{1}{(\sigma_1^y)^2} = G + H \;,\; 2F = \frac{1}{(\sigma_2^y)^2} + \frac{1}{(\sigma_3^y)^2} - \frac{1}{(\sigma_1^y)^2}$$

$$\frac{1}{(\sigma_2^y)^2} = H + F \;,\; 2G = \frac{1}{(\sigma_3^y)^2} + \frac{1}{(\sigma_1^y)^2} - \frac{1}{(\sigma_2^y)^2} \tag{6}$$

$$\frac{1}{(\sigma_3^y)^2} = F + G \;,\; 2H = \frac{1}{(\sigma_1^y)^2} + \frac{1}{(\sigma_2^y)^2} - \frac{1}{(\sigma_3^y)^2}$$

where σ_1^y, σ_2^y, and σ_3^y are the tensile yield stresses in the 1, 2, and 3 directions of anisotropy. Also, if τ_{23}^y, τ_{31}^y and τ_{12}^y are the yield stresses in shear with respect to the principal axes of anisotropy, then

$$2L = \frac{1}{(\tau_{23}^y)^2} \;,\; 2M = \frac{1}{(\tau_{31}^y)^2} \;,\; 2N = \frac{1}{(\tau_{12}^y)^2} \tag{7}$$

The form of Eq. (5) is valid only when the principal axes of anisotropy are taken to be the axes of reference; otherwise the stress components must be transformed in the manner described in

Appendix A. The functional dependence of the parameters of anisotropy on temperature and moisture follows from Eqs. (6) and (7) when the yield stresses are expressed as functions of temperature and moisture content.

The obvious association, implied by the term 'work-hardening,' between the work used to produce plastic flow and the hardening created, suggests the hypothesis that the degree of hardening is a function only of the total plastic work, and is otherwise independent of the strain path. The external work dW per unit volume done on the element during an infinitesimal increment of strain $d\varepsilon_{ij}$, with the continued loading of an element of the material is

$$dW = \sigma_{ij} d\varepsilon_{ij} \tag{8}$$

A part of this work

$$dW_e = \sigma_{ij} d\varepsilon^e_{ij} \tag{9}$$

represents recoverable elastic energy; the remainder is the plastic work per unit volume, i.e.,

$$\begin{aligned} dW_p = dW - dW_e &= \sigma_{ij}(d\varepsilon_{ij} - d\varepsilon^e_{ij}) \\ &= \sigma_{ij} d\varepsilon^p_{ij} \end{aligned} \tag{10}$$

where $d\varepsilon^p_{ij} = d\varepsilon_{ij} - d\varepsilon^e_{ij}$ is called the plastic strain increment. The term dW_p is necessarily positive since plastic distortion is an irreversible process, and the plastic work is then

$$W_p = \int \sigma_{ij} d\varepsilon^p_{ij} \tag{11}$$

In order for plastic work to be performed, the state of stress must be on the yield surface, i.e., the stress state must also satisfy the condition given by Eq. (5). To enforce this constraint, the Lagrange multiplier $d\lambda$ is used [67]. Then

$$\frac{\partial}{\partial \sigma_{ij}} [\sigma_{ij} d\varepsilon^p_{ij} - f(\sigma_{ij}) d\lambda] = 0 \tag{12}$$

which gives

$$d\varepsilon^p_{ij} = \frac{\partial f}{\partial \sigma_{ij}} d\lambda \tag{13}$$

With the use of Eq. (5), a set of equations for the plastic strain increments can then be written as follows:

$$\begin{aligned} d\varepsilon^p_{ij} &= \sigma^*_{ij} d\lambda, \quad i = j \\ d\gamma^p_{ij} &= 2\tau^*_{ij} d\lambda, \quad i \neq j \end{aligned} \tag{14}$$

where

$$\begin{aligned} \sigma^*_1 &= [H(\sigma_1 - \sigma_2) + G(\sigma_1 - \sigma_3)]/(F + G + H) \\ \sigma^*_2 &= [F(\sigma_2 - \sigma_3) + H(\sigma_2 - \sigma_1)]/(F + G + H) \\ \sigma^*_3 &= [G(\sigma_3 - \sigma_1) + F(\sigma_3 - \sigma_2)]/(F + G + H) \\ \tau^*_{23} &= L\tau_{23}/(F + G + H) \end{aligned} \tag{15}$$

$$\tau^*_{31} = M\tau_{31}/(F + G + H)$$

$$\tau^*_{12} = N\tau_{12}/(F + G + H)$$

Separating the strains into elastic and plastic components gives

$$\begin{aligned} d\varepsilon_1 &= S_{11}d\sigma_1 + S_{12}d\sigma_2 + S_{13}d\sigma_3 + d\varepsilon_1^p \\ d\varepsilon_2 &= S_{21}d\sigma_1 + S_{22}d\sigma_2 + S_{23}d\sigma_3 + d\varepsilon_2^p \\ d\varepsilon_3 &= S_{31}d\sigma_1 + S_{32}d\sigma_2 + S_{33}d\sigma_3 + d\varepsilon_3^p \end{aligned} \tag{16}$$

and for the shear components

$$\begin{aligned} d\gamma_{23} &= S_{44}d\tau_{23} + d\gamma_{23}^p \\ d\gamma_{31} &= S_{55}d\tau_{31} + d\gamma_{31}^p \\ d\gamma_{12} &= S_{66}d\tau_{12} + d\gamma_{12}^p \end{aligned} \tag{17}$$

where S_{ij} are the coefficients of the elastic compliance matrix $[S^e]$ in

$$\{d\varepsilon\} = [S^e]\{d\cdot\cdot \tag{18}$$

The inverse of Eq. (18) is

$$\{d\sigma\} = [C^e]\{d\varepsilon\} \tag{19}$$

where $[C^e]$ is the elastic stiffness matrix.

Relating the six parameters of anisotropy to the strain history is an extremely complicated problem. The problem can be simplified, however, by the assumption that the yield stresses must increase in proportion with strain hardening. This assumption is justified by the fact that the directions of anisotropy in fibrous composites remain effectively the same during deformation, and that for lack of experimental data, the choice of a complex hardening rule is not justified. If X_o, Y_o, etc., are the initial yield stresses, then according to the assumption of isotropic hardening above, $X = hX_o$, $Y = hY_o$, etc., where h is a parameter increasing monotonically from unity which expresses the amount of hardening. The anisotropic parameters must then decrease in accordance with Eq. (6) as $F = F_o/h^2$, etc. The way in which h varies with the strain can be explained by analogy with the isotropic theory due to von Mises. Let

$$\bar{\sigma}^2 = \frac{3}{2}\left[\frac{h^2}{F + G + H}\right]$$

$$= \frac{3}{2}\left[\frac{F(\sigma_2 - \sigma_3)^2 + G(\sigma_3 - \sigma_1)^2 + H(\sigma_1 - \sigma_2)^2}{F + G + H}\right.$$

$$\left. + \frac{2L\tau_{23}^2 + 2M\tau_{31}^2 + 2N\tau_{12}^2}{F + G + H}\right] \qquad (20)$$

be a nondimensional measure of the equivalent stress $\bar{\sigma}$. By analogy with the von Mises criterion for isotropic materials, Hill [10] suggested that if there is a functional relation between $\bar{\sigma}$ and the

work W (this is yet to be demonstrated by experiment), there must be one between $\bar{\sigma}$ and the effective (or equivalent) strain, $\int d\bar{\varepsilon}$, as defined by

$$d\bar{\varepsilon} = \left[\frac{2}{3}(F + G + H)\right]^{1/2}\left[\frac{F(Gd\varepsilon_2 - Hd\varepsilon_3)^2 + G(Hd\varepsilon_3 - Fd\varepsilon_1)^2 + H(Fd\varepsilon_1 - Gd\varepsilon_2)^2}{(FG + GH + HF)^2} + \frac{2(d\gamma_{23})^2}{L} + \frac{2(d\gamma_{31})^2}{M} + \frac{2(d\gamma_{12})^2}{N}\right]^{1/2} \tag{21}$$

where $d\varepsilon_{ij}$ and $d\gamma_{ij}$ are given by Eqs. (16) and (17). This is the analogue of the equivalent stress-equivalent strain curve for isotropic materials, the area under which is equal to the work per unit volume. Accordingly,

$$dW_p = \bar{\sigma}(d\bar{\varepsilon} - d\bar{\varepsilon}^e) = \bar{\sigma}d\bar{\varepsilon}^p \tag{22}$$

But, from Eq. (10)

$$dW_p = \sigma_1 d\varepsilon_1^p + \ldots + \tau_{23} d\gamma_{23}^p + \ldots \tag{23}$$

Substituting for $d\varepsilon_{ij}^p$ and $d\gamma_{ij}^p$ from Eq. (14) into Eq. (23) yields

$$dW_p = \frac{2}{3}\bar{\sigma}^2 d\lambda \tag{24}$$

If an effective stress-effective plastic strain curve is then constructed, the slope of such a curve at any point will be

$$H' = \frac{d\bar{\sigma}}{d\bar{\varepsilon}^p} \tag{25}$$

from which

$$d\bar{\varepsilon}^{p} = \frac{d\bar{\sigma}}{H'} \tag{26}$$

Now, substituting for $d\bar{\varepsilon}^{p}$ in Eq. (22), and equating the result to Eq. (24) since both are equal to the plastic work per unit volume dW_p,

$$\frac{\bar{\sigma}}{H'}\, d\bar{\sigma} = \frac{2}{3}\,\bar{\sigma}^{2}\, d\lambda = dW_p \tag{27}$$

Rearranging

$$\frac{2}{3}\,\bar{\sigma} d\bar{\sigma} = \frac{4}{9}\,\bar{\sigma}^{2}\, H' d\lambda \tag{28}$$

The left-hand side of Eq. (28) is recognized as the differential of Eq. (20), defining $\bar{\sigma}$. Thus,

$$\begin{aligned}\frac{2}{3}\,\bar{\sigma} d\bar{\sigma} = \frac{1}{F+G+H}\Big\{ & [-G(\sigma_3 - \sigma_1)d\sigma_1 + H(\sigma_1 - \sigma_2)d\sigma_1] \\ & + [F(\sigma_2 - \sigma_3)d\sigma_2 - H(\sigma_1 - \sigma_2)d\sigma_2] \\ & + [-F(\sigma_2 - \sigma_3)d\sigma_3 - G(\sigma_3 - \sigma_1)d\sigma_3] \\ & + 2L\tau_{23}d\tau_{23} + 2M\tau_{31}d\tau_{31} + 2N\tau_{12}d\tau_{12}\Big\}\end{aligned} \tag{29}$$

With the use of the definitions of Eq. (15), Eq. (29) can be rewritten as

$$\frac{2}{3}\bar{\sigma}d\bar{\sigma} = \sigma_1^* d\sigma_1 + \sigma_2^* d\sigma_2 + \sigma_3^* d\sigma_3$$

$$+ 2\tau_{23}^* d\tau_{23} + 2\tau_{31}^* d\tau_{31} + 2\tau_{12}^* d\tau_{12} \qquad (30)$$

To arrive at a relation between stress and strain, Eqs. (16) and (17) must be inverted. Rewriting these equations in matrix form,

$$\{d\varepsilon\} = [S^e]\{d\sigma\} + \{d\varepsilon^p\}$$

Thus,

$$[S^e]^{-1}\{d\varepsilon\} = [S^e]^{-1}[S^e]\{d\sigma\} + [S^e]^{-1}\{d\varepsilon^p\}$$

But $[S^e]^{-1} = [C^e]$. Also, because of the symmetry of $[S^e]$, $[S^e]^{-1}[S^e] = [I]$, where $[I]$ is the identity matrix. Hence, the above expression becomes

$$[C^e]\{d\varepsilon\} = \{d\sigma\} + [C^e]\{d\varepsilon^p\}$$

or

$$\{d\sigma\} = [C^e]\{d\varepsilon\} - [C^e]\{d\varepsilon^p\} \qquad (31)$$

Substituting from Eq. (14) for $d\varepsilon^p$,

$$\left\{\begin{matrix} d\sigma_{ii} \\ d\tau_{ij} \end{matrix}\right\} = [C_{ij}^e]\left\{\begin{matrix} d\varepsilon_{ii} \\ d\gamma_{ij} \end{matrix}\right\} - d\lambda[C_{ij}^e]\left\{\begin{matrix} \sigma_{ii}^* \\ 2\tau_{ij}^* \end{matrix}\right\}$$

or

$$\{d\sigma_{ij}\} = [C_{ij}^e]\{d\varepsilon_{ij}\} - d\lambda\{A\} \qquad (32)$$

where, for an orthotropic material, i.e., a material with three planes of symmetry,

$$\{A\} \equiv \begin{Bmatrix} C_{11}\sigma_1^* + C_{12}\sigma_2^* + C_{13}\sigma_3^* \\ C_{12}\sigma_1^* + C_{22}\sigma_2^* + C_{23}\sigma_3^* \\ C_{13}\sigma_1^* + C_{23}\sigma_2^* + C_{33}\sigma_3^* \\ 2C_{44}\tau_{23}^* \\ 2C_{55}\tau_{31}^* \\ 2C_{66}\tau_{12}^* \end{Bmatrix} \tag{33}$$

Equating Eqs. (28) and (30) yields

$$\frac{4}{9}\bar{\sigma}^2 H' d\lambda = \sigma_1^* d\sigma_1 + \sigma_2^* d\sigma_2 + \sigma_3^* d\sigma_3 + 2\tau_{23}^* d\tau_{23} + 2\tau_{31}^* d\tau_{31} + 2\tau_{12}^* d\tau_{12} \tag{34}$$

Now, substituting for $d\sigma$ in Eq. (34) from Eq. (32), and solving for $d\lambda$

$$d\lambda = \frac{A_1 d\epsilon_1 + A_2 d\epsilon_2 + A_3 d\epsilon_3 + A_4 d\gamma_{23} + A_5 d\gamma_{31} + A_6 d\gamma_{12}}{B} \tag{35}$$

where A_i ($i = 1, \ldots, 6$) are elements of $\{A\}$, and

$$B = \frac{4}{9}\bar{\sigma}^2 H' + A_1\sigma_1^* + A_2\sigma_2^* + A_3\sigma_3^* + 2A_4\tau_{23}^* + 2A_5\tau_{31}^* + 2A_6\tau_{12}^* \tag{36}$$

Finally, substituting for $d\lambda$ from Eq. (35) into Eq. (32) yields the desired form for the stress-strain relation

$$\{d\sigma\} = [C^P]\{d\varepsilon\} \tag{37}$$

where

$$[C^P] = \begin{bmatrix} C_{11}-\frac{A_1^2}{B} & C_{12}-\frac{A_1A_2}{B} & C_{13}-\frac{A_1A_3}{B} & -\frac{A_1A_4}{B} & -\frac{A_1A_5}{B} & -\frac{A_1A_6}{B} \\ & C_{22}-\frac{A_2^2}{B} & C_{23}-\frac{A_2A_3}{B} & -\frac{A_2A_4}{B} & -\frac{A_2A_5}{B} & -\frac{A_2A_6}{B} \\ & & C_{33}-\frac{A_3^2}{B} & -\frac{A_3A_4}{B} & -\frac{A_3A_5}{B} & -\frac{A_3A_6}{B} \\ & \text{Symmetric} & & C_{44}-\frac{A_4^2}{B} & -\frac{A_4A_5}{B} & -\frac{A_4A_6}{B} \\ & & & & C_{55}-\frac{A_5^2}{B} & -\frac{A_5A_6}{B} \\ & & & & & C_{66}-\frac{A_6^2}{B} \end{bmatrix} \tag{38}$$

is the plastic stiffness matrix.

3.5 Material Model

To apply the method of analysis developed in the previous section to fibrous composites, the material properties in the 1, 2, and 3 directions are needed. If the material is transversely isotropic, the properties in the 2 and 3 directions are the same. For mathematical consistency with the formulation, a relation between the effective stress and effective strain is required. Also, the tangent modulus H' of the effective stress-effective strain curve is needed, as shown in Eq. (36). Furthermore, the dependence of the material properties on temperature and moisture content is required if hygrothermal loadings are to be handled, and the actual material response under varying conditions of environment is to be considered. Both the elastic and the plastic response of a material change with temperature, and for polymeric materials, with moisture also, as evidenced by numerous experiments [6,16,17]. Therefore, the entire effective stress-effective strain curve of the material for each state of the environment must be available.

Ramberg and Osgood [22], used a three-parameter model to describe the stress-strain curve of a material. In their model, the strain was expressed as a function of the stress, with the three parameters selected to best fit the empirical data. Richard and Blacklock [68,69] developed another three-parameter model which was found to fit stress-strain curves for composite materials more accurately [19]. This model is of the form

$$\sigma = E\varepsilon/[1 + |E\varepsilon/\sigma_o|^n]^{1/n} \tag{39}$$

where σ_o and n are two independent parameters, and E is the initial slope of the stress-strain curve. Since the shape of an effective stress-effective strain curve is similar to a tensile stress-strain curve, a similar equation for the effective stress-effective strain can be written as

$$\bar{\sigma} = \bar{E}\,\bar{\varepsilon}/[1 + |\bar{E}\,\bar{\varepsilon}/\bar{\sigma}_o|^n]^{1/n} \tag{40}$$

where $\bar{\sigma}$ is the effective stress and $\bar{\varepsilon}$ is the effective strain, as defined by Eqs. (20) and (21), respectively. The two independent parameters $\bar{\sigma}_o$ and n, together with the third parameter $\bar{E}$, which is the initial slope of the curve, are selected to best fit the experimental data.

The tangent modulus H' of the effective stress-effective plastic strain curve is related to $\bar{E}$ as [70]

$$H' = \frac{\bar{E}\,\bar{E}_T}{\bar{E}-\bar{E}_T} \tag{41}$$

where $\bar{E}_T$ is found by differentiating Eq. (40) with respect to $\bar{\varepsilon}$. The resulting equation is

$$\bar{E}_T = \bar{E}/[1 + |\bar{E}\,\bar{\varepsilon}/\bar{\sigma}_o|^n]^{\frac{1+n}{n}} \tag{42}$$

By fitting Eq. (40) to the effective stress-effective strain curves for different temperatures and moisture contents, a functional relationship of the parameters $\bar{E}$, $\bar{\sigma}_o$, and n to temperature and moisture can be established. In a similar manner, functional relationships can also be found for all other material properties.

3.6 Finite Element Formulation

The finite element technique is now widely accepted as an accurate method of stress analysis. Progress has been made on three fronts, all of which contribute to the strength and flexibility of the method. First of all, the relation of the finite element method to previous well-established methods in continuum mechanics has given it a firm foundation. Secondly, the search for and development of the many types of finite elements that suit continuity and/or equilibrium requirements has given it a wide area of application. Finally, extension of the method to the study of both material and geometric nonlinearities has resulted in more realistic models and design methods.

Prior to the widespread application of digital computers, the inelastic behavior of solids was one of the most intractable problems in solid mechanics. The combination of large digital computers and the finite element method has made possible the solution of most of these hitherto intractable problems. However, in most of the previous literature on the subject, simple constant stress elements have been used. This was largely motivated by the

difficulty of performing an exact integration in an element containing both elastic and plastic regimes. With numerical integration techniques already introduced into the formulation of complex elements [71-73] in the analysis, such difficulties disappear. Among the different numerical integration techniques, the Gause method [70] is most widely used.

A recent comparison of various complex elements in three-dimensional analyses by Clough [74] has shown that isoparametric, numerically integrated brick elements are more efficient in elasto-plastic analyses than simple elements. An isoparametric formulation in three-dimensional space is presented in detail in Appendix B. This type of element, viz, the isoparametric element, will be used in the present work.

The data required to incorporate any element into a static analysis can be conveniently organized into four characteristic matrices. These matrices define the elastic or plastic behavior, the spatial assembly into the structure, and the required output information for each element. The four matrices are:

1) The element stiffness matrix, $[C^e]$ or $[C^p]$.
2) The element initial stress-free $\{F\}_{mo}$ or $\{d\}_{mo}$ vector.
3) The element assembly matrix.
4) The element output matrix.

The element initial stress-free vector depends on whether a stress field or a displacement field is assumed for the element.

For any type of element, a force-deformation relationship is needed, which leads to the first two characteristic matrices, i.e., the element stiffness matrix and the initial stress-free vector. The form of this relation is

$$\{F\}_m = [C]_m\{d\}_m - \{F\}_{mo} \tag{43}$$

where

$\{F\}_m$ = independent generalized forces for element m; a second subscript zero denotes initial values.

$[C]_m$ = element stiffness matrix (non-singular).

$\{d_m\}$ = independent generalized deformations for element m.

The third characteristic matrix is the element assembly matrix. To assemble the structural stiffness matrix in the assumed displacement method, which is used in this work, the independent deformation variables $\{d\}_m$ for each element have to be transformed into equivalent nodal displacements $\{\Delta\}_m$ in the global system, using the transformation (assembly) matrix $[a]_m$, i.e.,

$$\{d\}_m = [a]_m\{\Delta\}_m \tag{44}$$

Depending on whether the assumed displacement method or the assumed stress method is used, the fourth characteristic matrix relates the independent variables to the required output information, i.e., stresses in the former case, and displacements in the latter.

3.7 Computer Program

While the principles of three-dimensional elastic stress analysis by the finite element method have been obvious from the early days of the development of the method [75-77], their practical implementation leads to some immediate obstacles. As the number of elements increases, so do the number of degrees of freedom, increasing the size of the stiffness matrix, which requires larger computer in-core storage. In early approaches to three-dimensional analyses, the simple tetrahedral element was the obvious choice [76,78]. The adequacy of results of the two-dimensional simple triangle gave similar confidence in the tetrahedral element [79]. However, it was soon realized that, although convergence to the exact solution is guaranteed as the number of elements is increased, it was too slow for problems of even moderate size [80]. While the tetrahedron has certain advantages in its formulation [77], it is nevertheless an inconvenient shape to deal with in grid generating, i.e., topologically, and usually several have to be combined to form easily managed, hexahedral shapes [79]. Various families of isoparametric elements were introduced by Zienkiewicz, et. al., in 1967 [79]. These elements are more efficient than tetrahedrons, as mentioned earlier, and will be utilized in the present analysis, thus allowing a greater accuracy to be achieved for a given number of degrees of freedom and given computation time.

In the present work, a computer program has been developed making use of many of the more recent developments in both areas of

finite element analysis and computer programming. The following is a description of the main features of this program 'NCLAP' (Nonlinear Composite Laminate Analysis Program).

A modular approach has been adopted for NCLAP, with the various main finite element operations being performed by separate subroutines. Figure 5 shows the organization of the program. The basic finite element steps are performed by primary subroutines, which rely on auxiliary subroutines to carry out secondary operations. The construction falls into three phases.

Phase 1. Data are input and checked for possible preparation errors, an important feature when considering the amount of data input required for three-dimensional problems.

Phase 2. Stiffness and stress matrices and the applied load vector are generated. The nature of laminated composite problems requires elements with large aspect ratios, i.e., the ratio between minimum and maximum characteristic dimensions of an element in the mesh. This is because the thickness of a lamina is typically very small compared to its surface area. Large aspect ratios lead to an ill-conditioned stiffness matrix, i.e., the diagonal terms become very small compared to the off-diagonal terms, a situation that can lead to large solution errors. However, by using reduced integration techniques [81], the problem can be overcome.

Phase 3. A 'frontal' solution technique [82,83] is used for the solution of the stiffness equations. The advantages of using

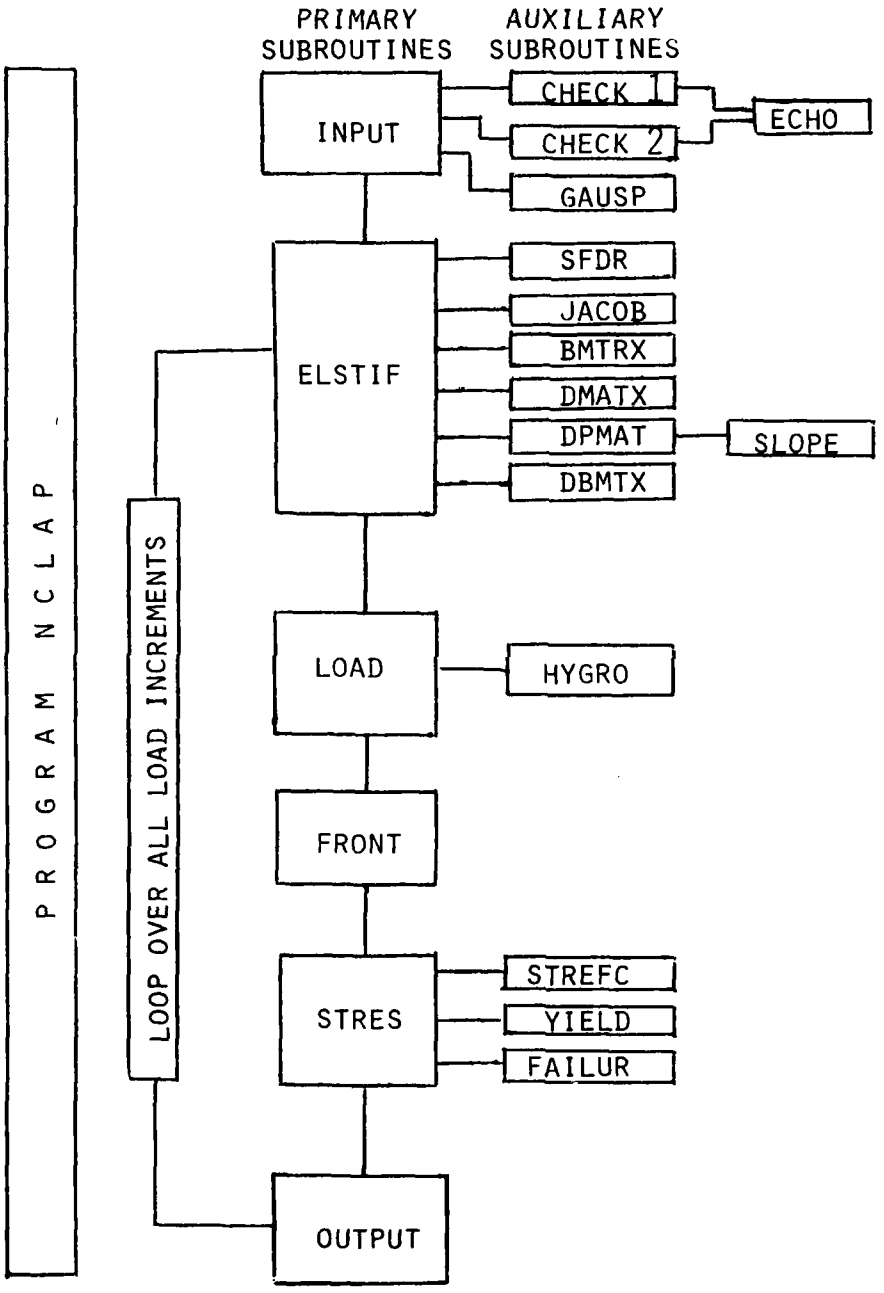

Figure 5. Organization Chart for Computer Program NCLAP

this method rather than the well-known banded matrix method are:

1) In solving the stiffness equations using a banded matrix, the order in which the nodes are numbered is very important since it influences the bandwidth. Using the frontal solution technique, however, does not require any ordering of nodal numbers. Hence, if a mesh is to be modified at a later time, no renumbering is needed. This saves considerable time and effort in data preparation.
2) For higher order elements, less core storage is needed. Several examples which justify this statement can be found in Reference [84].
3) Since variables are eliminated in this method as soon as conceivably possible, operations on zero coefficients are minimized and the total number of arithmetic operations is less than with other methods. Thus, less storage and computer time is used.
4) Because any new equation occupies the first available space in the front, there is no need for a bodily shifting of the in-core equations as in many other large capacity equation solvers.

In any incremental analysis, the use of smaller load increments implies a larger number of increments to achieve the same total applied load. Hence, more time is spent in reconstructing stiffness equations. A main feature of the computer program NCLAP developed in the present study is that it allows for the use of small load

increments without increasing the computing time significantly. The stiffness matrix is reconstructed only for those elements that become plastic, or when hygrothermal loading is considered.

A description of the input data required is given in Appendix D.

SECTION 4

EXAMPLE PROBLEMS

The method of analysis presented in this work, together with the computer program NCLAP developed for its implementation, can be applied to a very wide range of problems. This section illustrates a few of these possible applications. Four different problems will be solved using the analysis and, whenever possible, comparisons with results obtained using other methods will be made. These four problems cover the areas of generally orthotropic laminated beams and plates in bending, free edge effects in laminated plates, and the problems associated with these edge effects around circular holes. Both mechanical and hygrothermal loadings will be considered, and nonlinear material effects will be included.

4.1 Flexure of a Composite Beam Under Three-Point Loading

The problem of a composite beam under three-point loading is presented here and results are compared with results for the same problem using classical laminated plate theory as reported by Adams and Miller [85]. The composite beam is similar to an unnotched standard Charpy impact specimen, being simply supported, with a span s = 32.5 mm, and width b equal the height h = 6.5 mm, as shown in Figure 6. This beam consists of thirteen plies, with two plies at 0°, plies at +45° and -45°, two 0° plies, one ply at 90°, two plies at 0°, plies at -45° and +45°, and two 0° plies.

In accordance with the standard notation of Reference [7], the above composite laminate is identified as

$$[0_2/\pm 45/0_2/\overline{90}]_s$$

where the bar over the 90° ply indicates that the plane of symmetry passes through the middle of this ply. Symmetric laminates, such as the one presented, contain pairs of plies aligned at the same angle at equal distances on opposite sides of the midplane. For this type of laminate there is coupling between twisting curvatures and bending moments, i.e., the D_{16} and D_{26} terms in the [D] matrix of the classical laminated plate theory [4] are not zero.

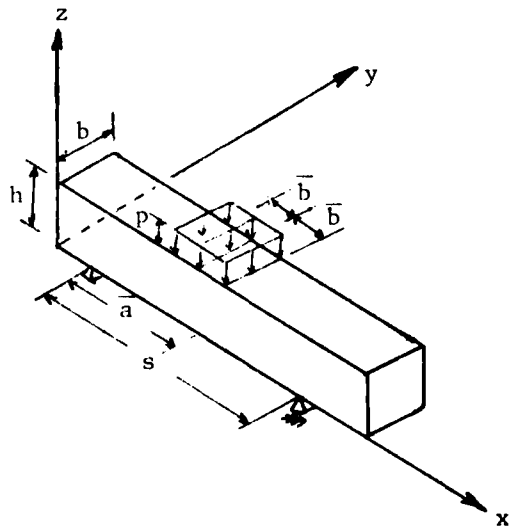

s = 32.5 mm
b = h = 6.5 mm

Figure 6. Simply Supported Beam Under Three-point Loading.

The material used was a Modulite 5206 graphite/epoxy composite [86], the mechanical properties of which are as follows:

$$E_{11} = 141\ GN/m^2\ (20.52\ Msi)$$

$$E_{22} = E_{33} = 15\ GN/m^2\ (2.15\ Msi)$$

$$G_{12} = G_{23} = G_{31} = 5.5\ GN/m^2\ (0.8\ Msi) \tag{45}$$

$$\nu_{12} = \nu_{23} = \nu_{31} = 0.25$$

The beam lay-up is shown in Figure 7, with the z-scale expanded to show detail. The three-dimensional finite element grid used consisted of ten layers of elements with six elements in the x-direction and one element in the y-direction in each layer. In this grid, the two 0° plies were treated as one layer and the 90° ply as two layers. The 90° ply was represented by two layers of elements so that the deflection at the midplane could be calculated and compared to that of Reference [85], since only midplane deflections could be calculated by the latter.

The load was applied as concentrated forces at the nodal points of the midspan, i.e., at $x = s/2$ as shown in Figure 7. A total force of 100 N (22.5 lb) was applied in the negative z-direction and the deflections at $x = s/2$, at each ply interface, were calculated. Table 1 gives the deflections at midspan for different values of z.

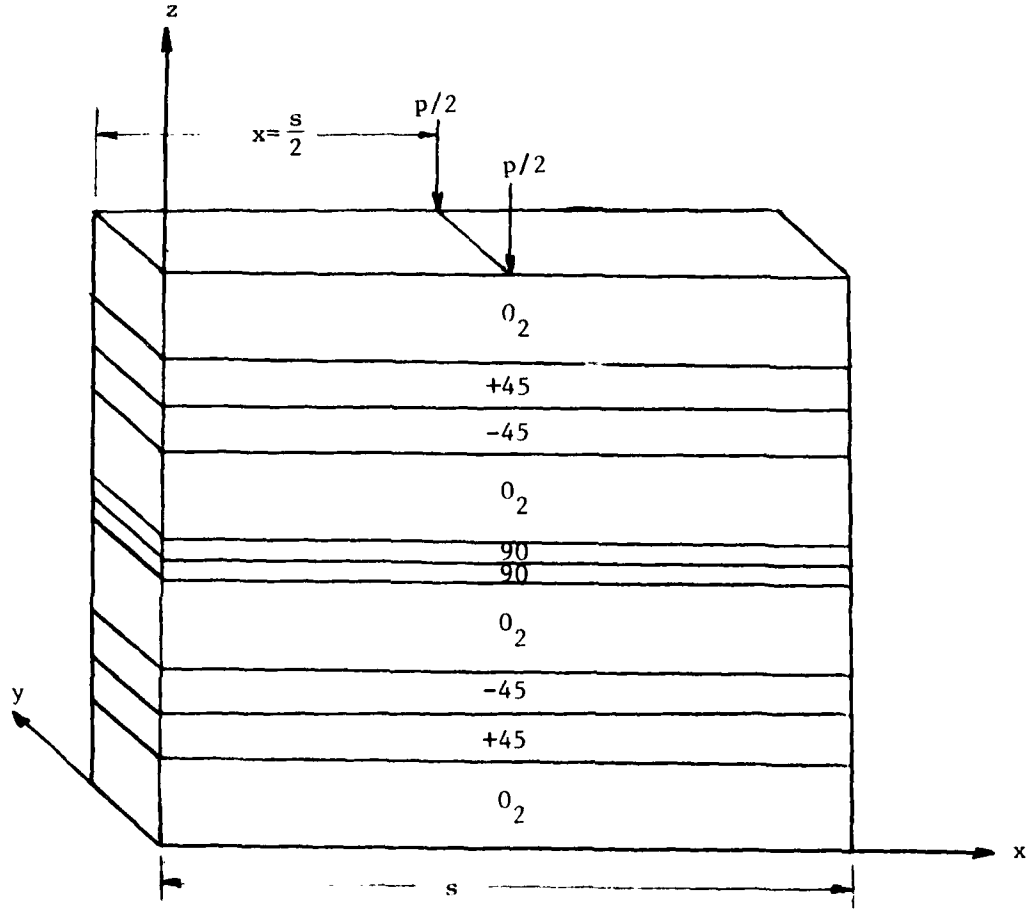

Figure 7. Layers of the Finite Element Grid for the Simply Supported Beam (z-scale expanded to show detail).

In the study by Adams and Miller [85], the classical laminated plate theory was used to solve the same problem, viz, bending of a composite beam under three-point loading (Figure 6). They assumed a double sine series for the load in the form

$$p_m = \frac{4p_o}{m\pi} \sin \frac{m\pi\bar{a}}{s} \sin \frac{m\pi\bar{b}}{s} \tag{46}$$

where p_o is the load intensity, $\bar{a}$ is the location of the center of application of the load, and $2\bar{b}$ is the length of the beam over which the load is applied. The value of 0.02s was used for $\bar{b}$ to approximate a concentrated load at midspan, as illustrated in Figure 6. They obtained a solution for the deflection w in the form

$$w = \sum_m \frac{p_m s^2}{m^2\pi^2}\left(\frac{1}{k_1^2 A_{55}} + \frac{s^2}{m^2\pi^2 D_{11}}\right)\sin \frac{m\pi x}{s} \tag{47}$$

in which A_{55} and D_{11} are terms of the well-known [A] and [D] matrices of the classical laminated plate theory [4], and k_1 is an experimentally determined shear correction factor. For the laminate of this example, these values are [85]

$$A_{55} = 36.8 \text{ MNm}^{-1} (2.1 \times 10^5 \text{ lb in}^{-1})$$

$$D_{11} = 3.2 \text{ kN-m } (2.8 \times 10^4 \text{ in-lb})$$

$$k_1 = 0.66$$

Using the method of Reference [85], as described above, only the deflection at the midplane ($z = h/2$) can be calculated; the maximum deflection at midspan, as calculated from Eq. (47), is

$$w_{max} = -7.760\mu m \ (-0.306 \times 10^{-6} \text{ in}) \tag{48}$$

This value corresponds to the value at $z = 3.25$ mm in Table 1, which is

$$w\Big|_{z=h/2} = -8.034\mu m \ (-0.316 \times 10^{-6} \text{ in}) \tag{49}$$

The theory of Reference [85], as represented by the value given in Eq. (48), was shown to predict values of deflection somewhat lower than obtained experimentally. Thus, the present analysis, represented by Eq. (49), is actually in better agreement with available experimental data, possibly due to the fact that the D_{16} and D_{26} terms were neglected in the analysis of Reference [85].

Table 1 also shows the effect of interlaminar stresses on the deflection of the midspan. The midspan deflection is not the same at each ply interface; rather there is a change in the thickness of each lamina due to the concentrated applied load at midspan. This effect cannot be detected by the classical laminated plate theory, and is not predicted by Reference [85]. The magnitude of the maximum interlaminar normal stress σ_z is 8 percent of the maximum in-plane stress σ_x for this example. This is a significant value, since the transverse stiffness is only 4 percent of the

Table 1. Midspan Deflections of a Simply Supported $[0_2/\pm 45/0_2/\overline{90}]_s$ Laminated Composite Beam Under Three-Point Loading as Predicted by the 3-D Finite Element Analysis (NCLAP)

Distance from Bottom Surface z (mm)	Deflection w (-μm)
0.0	7.726
1.0	7.766
1.5	7.797
2.0	7.843
3.0	7.986
3.25	8.034

longitudinal stiffness. The effects of interlaminar stresses will be discussed in more detail in the last two examples.

4.2 Cylindrical Bending of Laminated Plates

In the past, laminated plates have often been analyzed using the assumption that they behaved as specially orthotropic laminates. For this type of laminate, the D_{16} and D_{26} terms of the [D] matrix are zero. Most practical laminates, however, do not fulfill these conditions of special orthotropy.

Unlike other methods in the literature, the method of analysis presented in the present work can handle any lay-up and is not restricted to symmetric or specially orthotropic laminates. To be able to check the results of the present computer program, however, problems reported in the literature are modeled and results compared. One such problem is that of cylindrical bending of an antisymmetric, specially orthotropic (cross-ply) laminated plate.

Shown in Figure 8 is the three-dimensional grid used to model an antisymmetric laminated plate of the configuration $[0/90/0/90]_T$. The plate is 30 mm long, 20 mm in width, and consists of four plies each of which is 0.4 mm thick. Each ply is represented by a layer of 24 elements, with 6 elements in the x-direction, and 4 in the y-direction. Thus, the grid consists of a total of 96 elements, 175 nodes and 525 degrees of freedom.

The plate is simply supported along x = 0 and x = a and is free along the other two edges (see Figure 8). A constant transverse

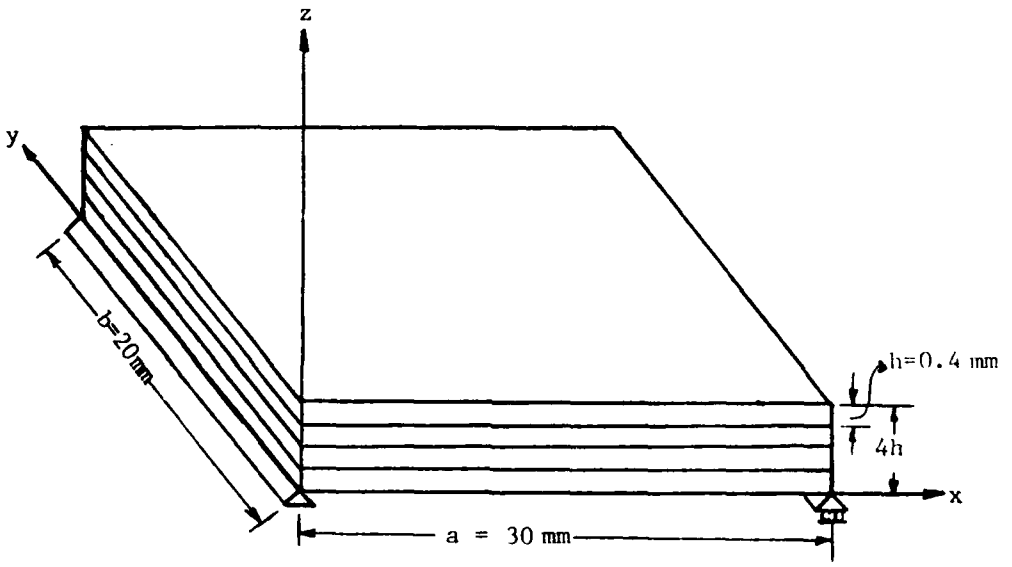

Figure 8. Four-ply Laminated Plate

load q_o is applied by means of nodal forces. Each node on the top surface is loaded by a 1N (0.225 lb) force in the negative z-direction, corresponding to a uniform transverse applied load of q_o = 0.16 MPa (23.2 psi). The maximum deflection at the center of the plate as calculated by NCLAP is

$$w\Big|_{z=2h} = -0.0492 \text{ mm } (-1.9370 \times 10^{3} \text{ in}) \tag{50}$$

The same problem was also solved using the classical laminated plate theory solution presented in Reference [5], which is based on the assumptions that the plate is of infinite length in the y-direction and that the transverse load is independent of y, i.e., q = q(x). Thus, the deformed surface will be cylindrical, i.e.,

$$u_o = u_o(x), \quad v_o = 0, \quad w = w(x) \tag{51}$$

where u_o and v_o are the midplane displacements in the x and y directions, respectively. According to Reference [5], the maximum deflection occurs at the center of the plate and is given by

$$w_{max} = \frac{5A_{11}q_o a^4}{384\ D} \tag{52}$$

where

$$D = A_{11}D_{11} - B_{11}^2 \tag{53}$$

and w does not vary with z, as indicated by Eq. (51).

With the aid of the computer program AC3, which is a point stress analysis program [7], the [A], [B], and [D] matrices of the classical laminated plate theory were evaluated for the $[0/90/0/90]_T$ configuration. Using Eqs. (52) and (53), the maximum deflection was then calculated as

$$w_{max} = -0.0653 \text{ mm } (2.5708 \times 10^{-3} \text{ in}) \qquad (54)$$

As calculated by the present program, displacements in the y-direction, i.e., v_o, satisfied Eq. (51). Displacements in the x-direction, however, showed dependence on the other two coordinates, i.e., $u = u(x,y,z)$. At this point, the difference between the value of w in Eqs. (50) and (54) cannot be adequately explained.

The w deflection variation along $x = a/2$ is given in Table 2, at every ply interface. A slight decrease in w occurs away from the boundaries $y = 0$ and $y = b$. This change of w at the boundaries is caused by the edge effects due to the presence of interlaminar stresses. It does not exist for laminates with no interlaminar stresses, e.g., isotropic laminates. The significance of interlaminar stresses will be discussed in the following examples.

4.3 Interlaminar Stresses in Laminated Plates

As stated earlier, laminated composites develop out-of-plane or interlaminar stresses even under uniaxial loading. It was also shown that these stresses cause delamination of the laminate. Two-dimensional analyses presented in the literature cannot accurately

Table 2. Plate Deflections Under Uniform Transverse Load Along x = a/2, as Predicted by the 3-D Finite Element Analysis (NCLAP)

Distance from Bottom Surface z (mm)	Deflection w (mm) at Values of y/b Indicated				
	0.0	0.25	0.50	0.75	1.0
0.0	0.0492	0.0489	0.0488	0.0489	0.0492
0.4	0.0492	0.0489	0.0489	0.0489	0.0492
0.8	0.0492	0.0489	0.0489	0.0489	0.0492
1.2	0.0492	0.0489	0.0489	0.0489	0.0492
1.6	0.0492	0.0489	0.0488	0.0489	0.0492

handle the problem of interlaminar stresses, since this problem is three-dimensional in nature. Results obtained with these methods will be compared to results using the present analysis in the following example.

Four-ply symmetric laminates will be considered. Because of symmetry, only one quarter of the upper two plies of the plate need be considered, as shown in Figure 9. The origin is therefore at the midplane. The three-dimensional finite element grid used consisted of two layers of elements. Each layer, being 30 mm in the x-direction and 20 mm in the y-direction (see Figure 9), was constructed by six elements in the x-direction and four in the y-direction. Ply thickness was taken to be 0.4 mm; thus a b/h ratio of 50 was achieved, where b is the width of the plate in the y-direction and h is the lamina thickness.

To show an important and useful feature of the present analysis, viz, the ability to handle hygrothermal as well as mechanical loadings, or even a combination of these two types of loadings, the material properties over a range of temperature and moisture levels must be known. Few data have been published that describe the dependence of material properties on environmental changes. One such set of data available is for the Hercules AS/3501-6 unidirectional graphite/epoxy composite, which will be used in this example. The functional dependence of the properties of this material on temperature and moisture were experimentally

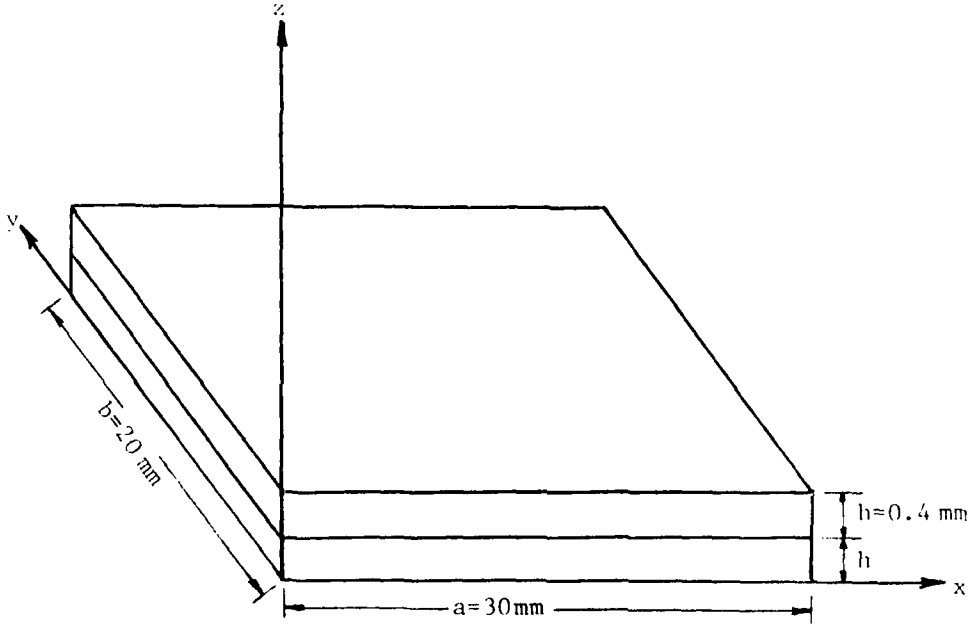

Figure 9. One Quadrant of the Upper Two Plies of a Four-Ply Composite Laminate.

determined at the University of Wyoming [87]. These properties are represented by the second order polynomial

$$P(T,M) = C_1T^2 + C_2M^2 + C_3T\cdot M + C_4T + C_5M + C_6 \qquad (55)$$

where P is the functional material property of interest, T is temperature (°C), M is moisture content (weight percent), and the C's are coefficients given in Table 3.

Although the present method can handle both applied nodal forces and displacements, most analyses presented in the literature can only handle uniaxial strain. For this reason, i.e., to be able to compare results, the same type of loading, viz, uniaxial strain was used here. For each laminate considered, a uniform displacement was applied in the x-direction such that $\bar{\varepsilon}_x = 0.01$ percent. The average in-plane stress $\bar{\sigma}_x$ is also given for each case. This will permit the comparison of the relative magnitudes of the applied in-plane stresses to the interlaminar stresses,to ascertain the importance of the latter.

4.3.1 Cross-Ply Laminates

The interlaminar stress distributions for $[90/0]_s$ and $[0/90]_s$ laminates are shown in Figure 10. The interlaminar normal stress σ_z, plotted in Figure 10a, is very small at y/b = 0. As y/b increases toward the free edge of the plate, σ_z increases (in absolute sense) to a peak value, then reverses direction. This peak value occurs at y/b = 0.5 for the $[90/0]_s$ laminate, and at

Table 3. Coefficients of Polynomials in Eq. (55) for the Mechanical Properties of Hercules AS/3501-6 Unidirectional Graphite/ Epoxy Composite [87]

Material Property (MPa)	C_1	C_2	C_3	C_4	C_5	C_6
E_{11}	-0.424	-1.357	-1.329	-13.66	8.781	$1.301\ (10^{3})$
E_{22}	-0.164	-0.211	-0.133	-10.97	0.121	$1.119\ (10^{4})$
E_{33}	-0.164	-0.211	-0.133	-10.97	0.121	$1.119\ (10^{4})$
G_{23}	-0.046	-0.095	$1.33\ (10^{-4})$	-5.451	-4.035	$3.748\ (10^{3})$
G_{31}	-0.086	-0.178	$2.50\ (10^{-4})$	-10.23	-7.570	$7.031\ (10^{3})$
G_{12}	-0.086	-0.178	$2.50\ (10^{-4})$	-10.23	-7.570	$7.031\ (10^{3})$
σ_1^y	$-3.095\ (10^{-3})$	$-6.807\ (10^{-3})$	$-3.000\ (10^{-3})$	-0.477	-0.067	776.1
σ_2^y	$-7.211\ (10^{-4})$	$-1.276\ (10^{-3})$	$1.372\ (10^{-3})$	-0.148	-0.158	52.4
σ_3^y	$-7.211\ (10^{-4})$	$-1.276\ (10^{-3})$	$1.372\ (10^{-3})$	-0.148	-0.158	52.4
τ_{23}^y	$-3.171\ (10^{-4})$	$-6.468\ (10^{-4})$	$-9.800\ (10^{-4})$	$5.360\ (10^{-3})$	0.037	30.7
τ_{31}^y	$-7.387\ (10^{-5})$	$-1.507\ (10^{-4})$	$-2.283\ (10^{-4})$	$1.249\ (10^{-3})$	$8.679\ (10^{-3})$	7.153
τ_{12}^y	$-7.387\ (10^{-5})$	$-1.507\ (10^{-4})$	$-2.283\ (10^{-4})$	$1.249\ (10^{-3})$	$8.697\ (10^{-3})$	7.153
σ_1^u	$-5.881\ (10^{-3})$	$-1.705\ (10^{-2})$	$-7.508\ (10^{-3})$	-0.206	0.321	1467.0
σ_2^u	$-5.892\ (10^{-4})$	$-1.792\ (10^{-3})$	$1.431\ (10^{-3})$	-0.163	-0.189	60.7
σ_3^u	$-5.892\ (10^{-4})$	$-1.792\ (10^{-3})$	$1.431\ (10^{-3})$	-0.163	-0.189	60.7
τ_{23}^u	$-9.130\ (10^{-4})$	$-8.208\ (10^{-4})$	$1.482\ (10^{-3})$	-0.141	-0.139	87.3
τ_{31}^u	$-9.146\ (10^{-5})$	$-8.222\ (10^{-5})$	$1.485\ (10^{-4})$	-0.014	-0.014	8.746
τ_{12}^u	$-9.146\ (10^{-5})$	$-8.222\ (10^{-5})$	$1.485\ (10^{-4})$	-0.014	-0.014	8.746

Table 4. Poisson's Ratio, and Thermal and Moisture Expansion Coefficients for Hercules AS/3501-6 Unidirectional Graphite/Epoxy Composite [87]

ν_{23}	0.492	
ν_{13}	0.308	
ν_{12}	0.308	
α_{11}	0.882	$10^{-6}/°C$
α_{22}	30.6	$10^{-6}/°C$
α_{33}	30.6	$10^{-6}/°C$
β_{11}	90.0	$10^{-6}/\%M$
β_{22}	3.0	$10^{-3}/\%M$
β_{33}	3.0	$10^{-3}/\%M$

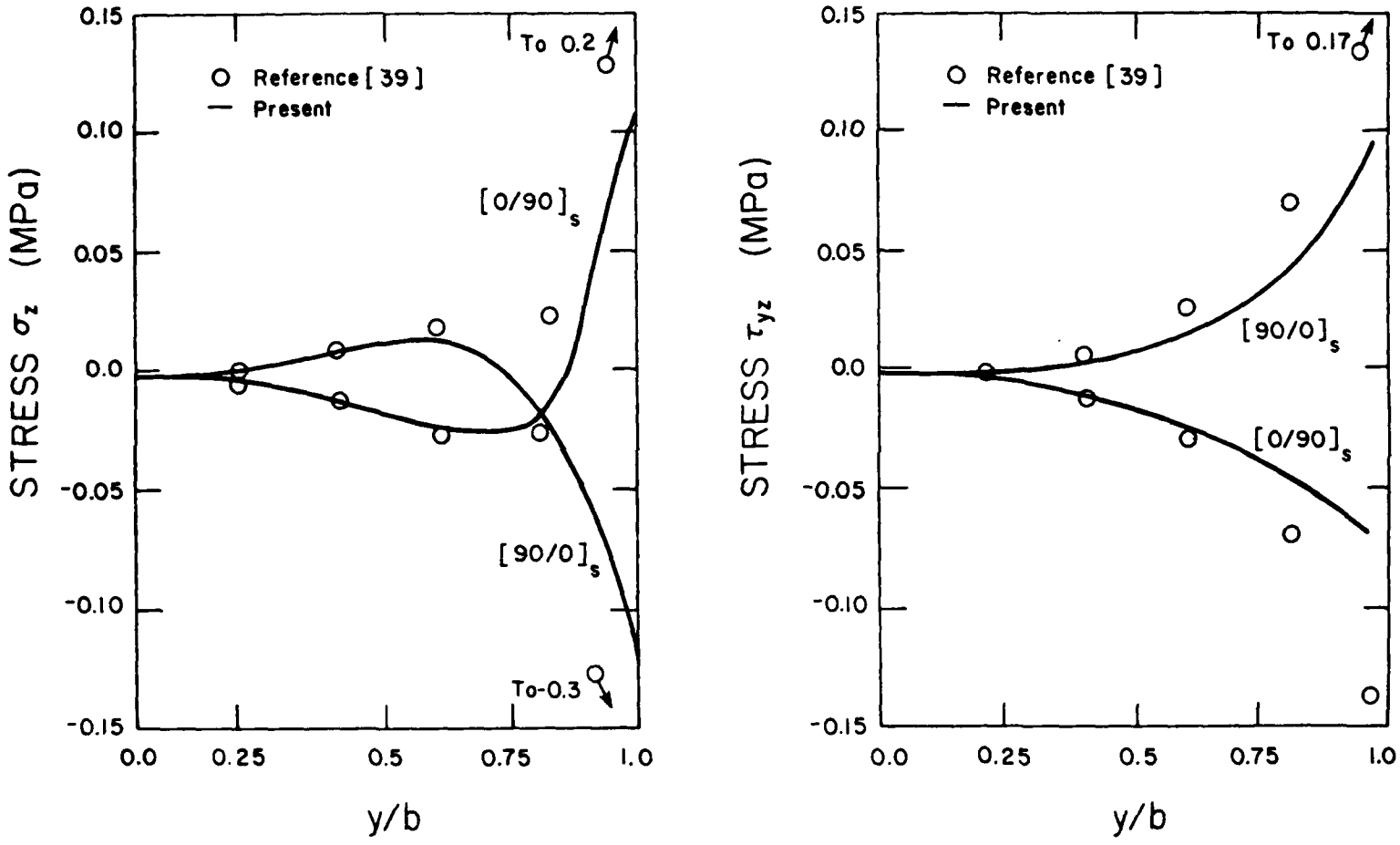

Figure 10. Interlaminar Stresses at Midplane for $[0/90]_s$ and $[90/0]_s$ Laminates Under Uniaxial Strain $\bar{\varepsilon}_x = 0.01\%$ ($\bar{\sigma}_x = 7.1$ MPa).

y/b = 0.75 for the $[0/90]_s$ configuration, i.e., closer to the free edge in the latter configuration. The peak value of σ_z for the $[0/90]_s$ laminate is almost double that reached in the $[90/0]_s$ laminate. At y/b = 0.96, the interlaminar normal stress shows a high but finite value; tension in the $[0/90]_s$ configuration and compression in the $[90/0]_s$ laminate. Thus, the distribution of the interlaminar normal stress in the $[0/90]_s$ laminate is not a mirror image of the distribution in the $[90/0]_s$ laminate. This behavior agrees with results recently reported by Spilker and Chou [88] in their work on interlaminar stresses. A slightly different graphite/epoxy material was used in their work, e.g., the longitudinal modulus $E_{11} = 1.4 \times 10^5$ MPa as compared to a value of 1.2×10^5 MPa for the Hercules AS/3501-6 material used in this example. The purpose here, however, is to show the trend in the material behavior rather than a point-by-point stress comparison. Spilker and Chou also reported that satisfying the traction-free edge condition, i.e., the boundary conditions at the free boundaries, would result in the convergence of all stresses to finite values at the free edge, in direct conflict with the idea of stress singularities [39,40]. To satisfy the traction-free edge condition, special elements must be used, such as those of Reference [88], or the hybrid elements of Reference [79]. These are complex elements, however, and Reference [88] shows that satisfying the traction-free edge conditions, while giving more accurate point-by-point stress values, does not change the stress gradient.

As shown in Figure 10b, the interlaminar shear stress distribution τ_{yz} for the $[0/90]_s$ laminate is also not a mirror image of that for the $[90/0]_s$ laminate. The interlaminar shear stress τ_{yz} increases in absolute value from y/b = 0 to y/b = 0.96, where it reaches a peak value near the free edge, then drops to zero at the free boundary (y/b = 1.0), as dictated by the traction-free boundary condition.

Figure 11 is a plot of the interlaminar normal stress σ_z through the thickness. To increase information about the distribution through the thickness, the finite element grid was changed for the plot of Figure 11. Each ply was represented by two layers of elements instead of one. It is again noted that the stress distribution for the $[90/0]_s$ laminate is not a mirror image of that for the $[0/90]_s$ laminate. Near the free edge, the interlaminar normal stress has a maximum value at the midplane of both configurations, i.e., at z/h = 0, as shown in Figure 11. These results are in good agreement with those reported by Wang and Crossman [39].

In order to permit comparison with other published results, the same problems were solved again using the material properties of Reference [24], which are given below.

E_{11} = 138 GPa (20 Msi)

$E_{22} = E_{33}$ = 14.5 GPa (2.1 Msi)

$G_{23} = G_{31} = G_{12}$ = 6 GPa (0.85 Msi)

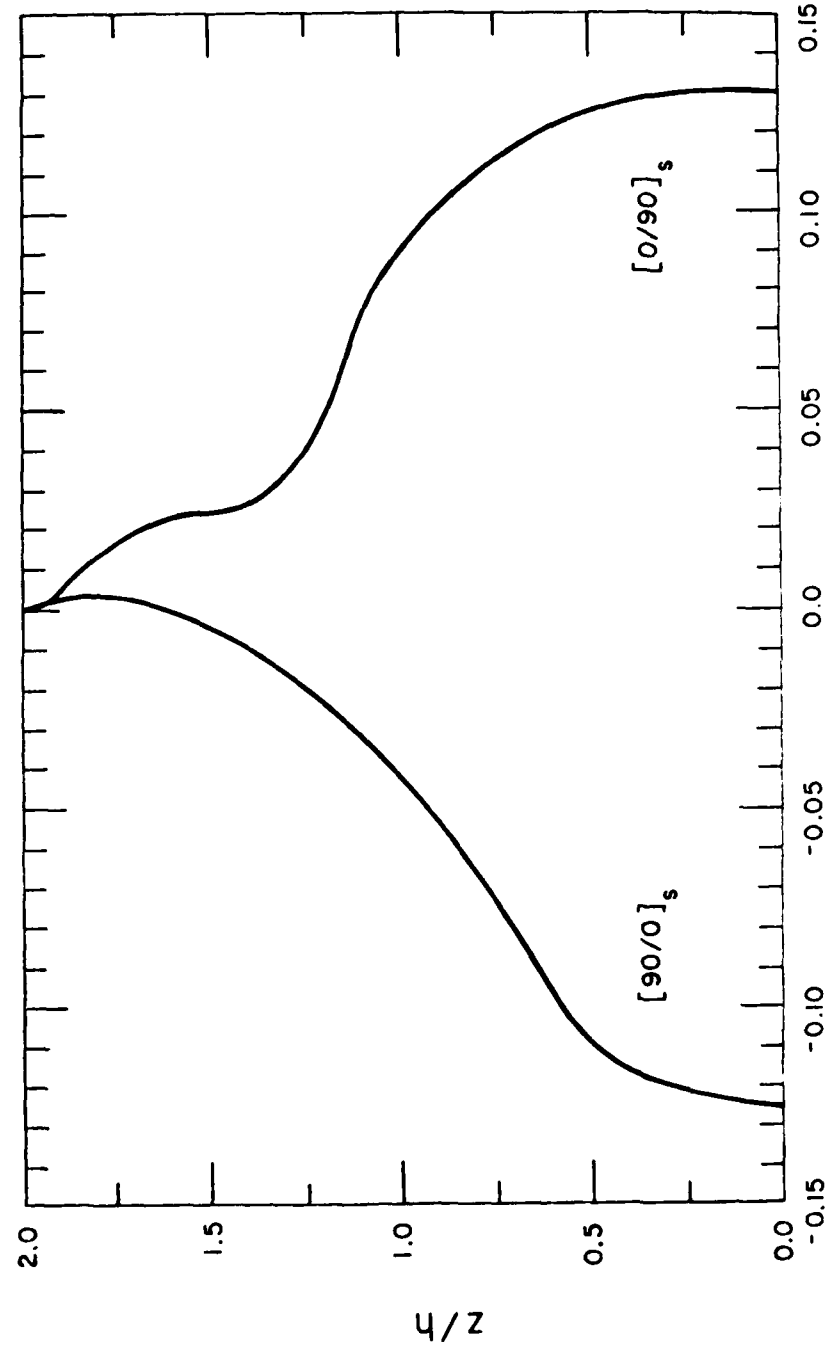

Figure 11. Through the Thickness Distribution of the Interlaminar Stress Near the Free Edge of $[0/90]_s$ and $[90/0]_s$ Laminates Subjected to Uniaxial Strain $\bar{\varepsilon}_x = 0.01\%$ ($\bar{\sigma}_x = 7.1$ MPa).

$$\nu_{23} = \nu_{31} = \nu_{12} = 0.21$$

Distributions of σ_z and τ_{yz} at z/h = 1 for the $[0/90]_s$ and $[90/0]_s$ configurations were calculated. For the $[0/90]_s$ laminate, the present results agreed well with those reported by Renieri and Herakovich [24]. Both methods predicted that for y/b < 0.5, the classical laminated plate theory solution was approximately recovered. The maximum value of σ_z near the free edge as calculated with the present three-dimensional analysis was the same as that of Reference [24]. This value was much smaller, however, than that reported by Wang and Crossman [39] using the same material. Basically, the results of the present work and those reported in References [24,39,88] were close up to y/b = 0.5; but in regions nearer the free edge, results differed. While Wang and Crossman [39] indicated a zero value for σ_z at the free edge, both the present method and that of Renieri and Herakovich [24] predicted the value of σ_z close to the free edge to be compression. The conclusions stated above for σ_z were found to be true also for the interlaminar shear stress distributions. For the $[90/0]_s$ configuration, the present results again agreed well with those of Reference [24] for both components of interlaminar stress.

4.3.2 Angle-Ply Laminates Under Mechanical and Hygrothermal Loading

Angle-ply laminates of the configuration $[\pm\theta]_s$, and $[\overline{+}\theta]_s$, where θ is the ply angle, were also considered here, results being

presented in Figures 12-14 for $\theta = 20°$, $30°$, and $70°$. The following observations apply to each of these configurations.

The interlaminar normal stress σ_z at midplane for the $[\pm\theta]_s$ laminates increases from compression at $y/b = 0$ to tension at $y/b = 1$, i.e., at the free edge. For the $[\mp\theta]_s$ laminates, σ_z decreases from tension at $y/b = 0$ to compression at the free edge. The absolute value of σ_z at $y/b = 0$ for the $[\pm\theta]_s$ configurations is about half that for the $[\mp\theta]_s$ configurations.

Results presented here are in disagreement with those reported by Pipes and Pagano [26], who noted that the presence of interlaminar stresses might be considered an edge effect restricted to a small region near the free edge. In their work of Reference [26], Pipes and Pagano presented a method for predicting the interlaminar stresses under uniform axial extension. They considered symmetric angle-ply laminates loaded by tractions applied only on the ends x = constant. A displacement field of the form

$$\begin{aligned} u &= Cx + U(y,z) \\ v &= V(y,z) \\ w &= W(y,z) \end{aligned} \tag{56}$$

was then assumed. This type of displacement field, together with the symmetry conditions, led to the following boundary conditions:

$$\begin{aligned} \gamma_{xz}(y,0) &= 0 \\ \gamma_{yz}(y,0) &= 0 \end{aligned} \tag{57}$$

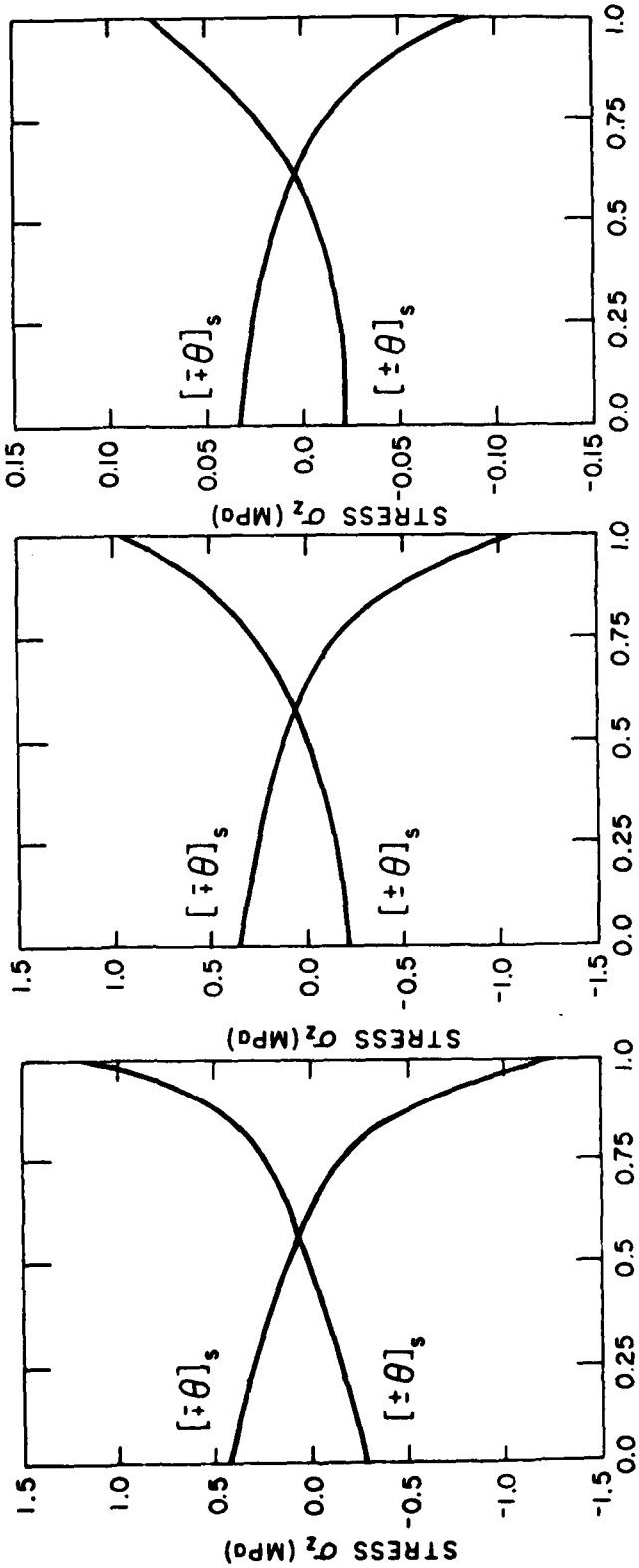

a) $\theta = 20°$, $\bar{\sigma}_x = 9.1$ MPa
b) $\theta = 30°$, $\bar{\sigma}_x = 5.5$ MPa
c) $\theta = 70°$, $\bar{\sigma}_x = 1.2$ MPa

Figure 12. Interlaminar Normal Stress at the Midplane for $[\pm\theta]_s$ and $[\pm\theta]_s$ Laminates Subjected to a Uniaxial Strain $\bar{\epsilon}_x = 0.01\%$.

$$\gamma_{yz}(0,z) = 0$$

Pipes and Pagano [26] noted that such an analysis, which considers stress boundary conditions only, cannot handle a bar with clamped ends under extension, such as a tensile coupon, and that their method was simply an attempt to discern the influence of a free edge on laminate response. They stated that the true behavior can only be studied by abandoning the assumption that all stress components are independent of x. Most of the methods of analysis presented in the literature, however, have taken the same approach as Pipes and Pagano [26] in dealing with the problem of interlaminar stresses. It is believed that the differences between the results of Reference [26] and those of the present analysis, which includes the dependence on x, are due to the assumptions used in Reference [26], as discussed above.

The interlaminar shear stress τ_{yz}, presented in Figure 13 for different values of θ, is always positive for the $[\bar{+}\theta]_s$ laminates, in agreement with results for a $[\bar{+}45]_s$ laminate reported by Rybicki [34]. The plots of τ_{yz} shown in Figure 13 indicate a steady increase (or decrease) to a high absolute value near the free edge before reaching zero at y/b = 1, as dictated by the traction-free edge condition. This high value of τ_{yz} near the free edge was also reported by Pipes and Pagano [26]. The variation in the interlaminar shear stress τ_{zx}, as shown in Figure 14, is less than the variation in τ_{yz}.

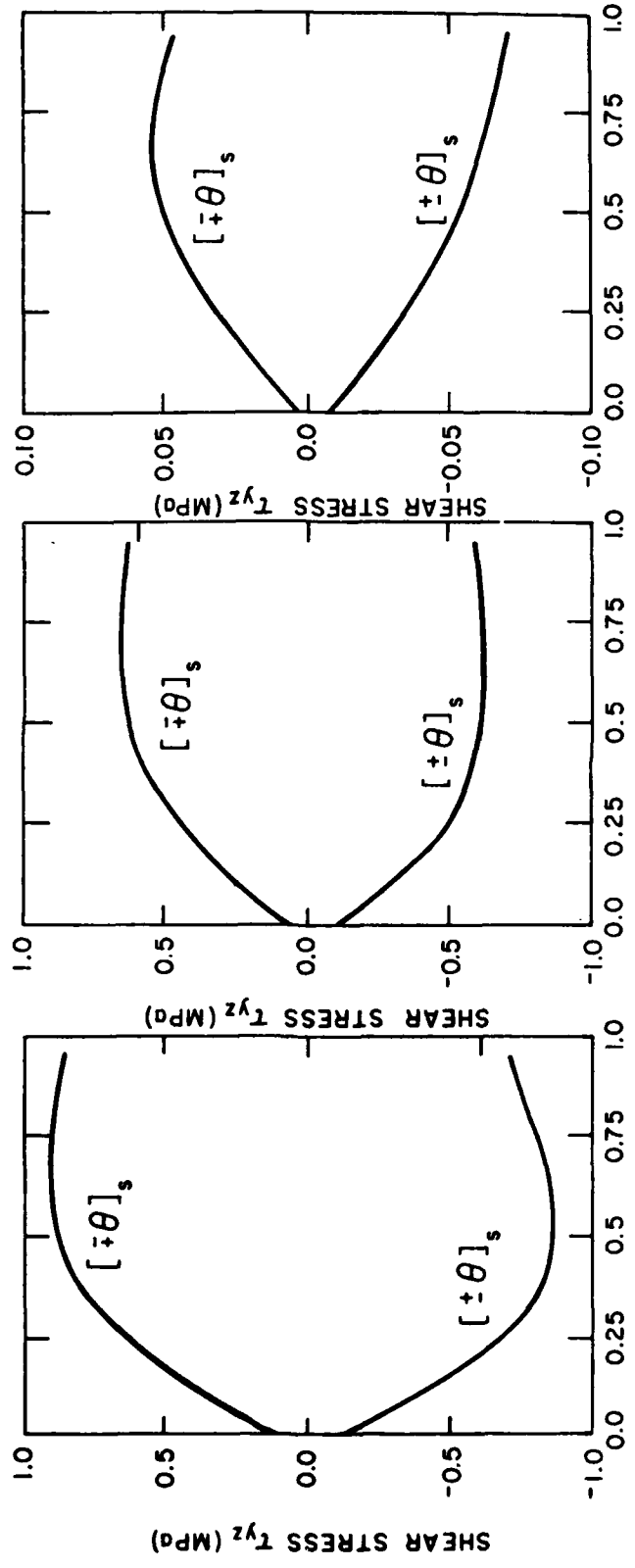

a) $\theta = 20°$, $\bar{\sigma}_x = 9.1$ MPa b) $\theta = 30°$, $\bar{\sigma}_x = 5.5$ MPa c) $\theta = 70°$, $\bar{\sigma}_x = 1.2$ MPa

Figure 13. Interlaminar Shear Stress at the Midplane for $[\pm\theta]_s$ and $[\mp\theta]_s$ Laminates Subjected to a Uniaxial Strain $\bar{\varepsilon}_x = 0.01\%$.

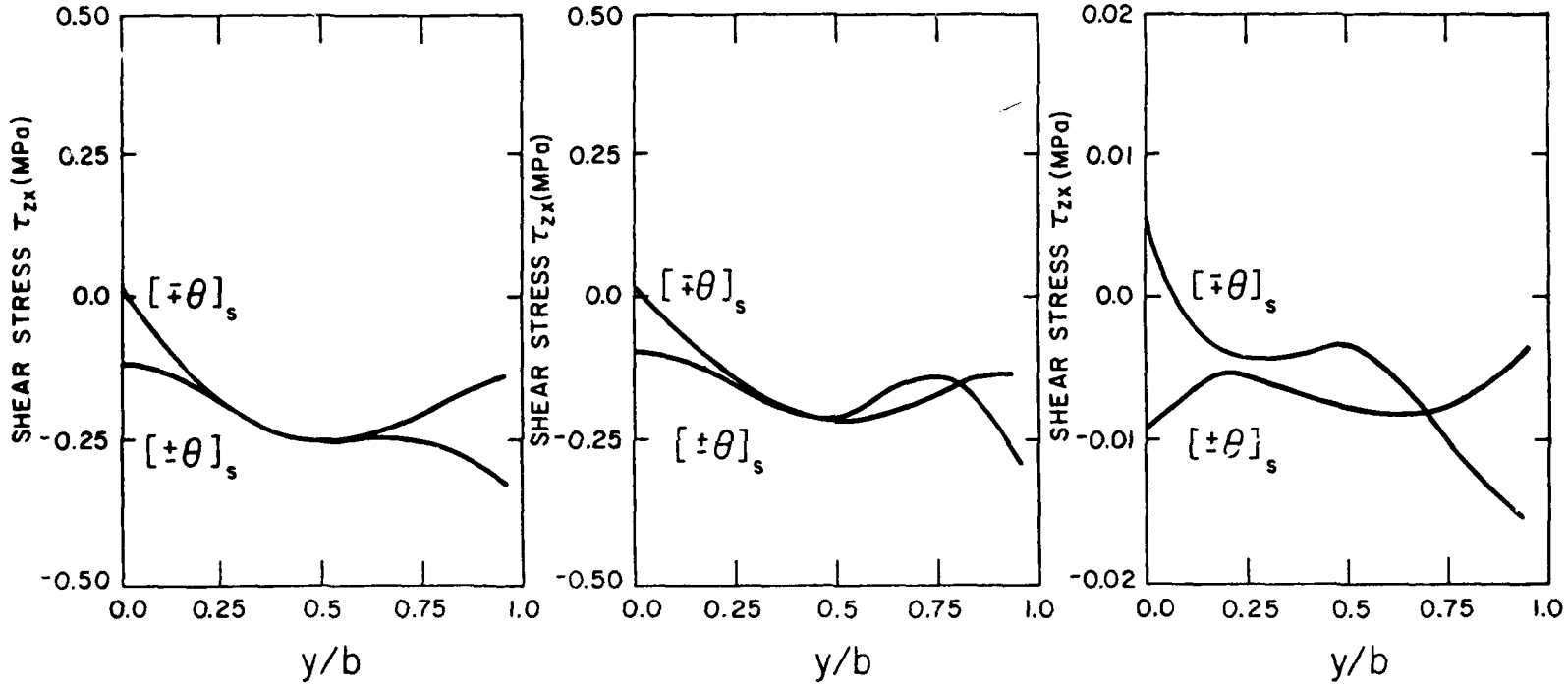

a) $\theta = 20°$, $\bar{\sigma}_x = 9.1$ MPa b) $\theta = 30°$, $\bar{\sigma}_x = 5.5$ MPa c) $\theta = 70°$, $\bar{\sigma}_x = 1.2$ MPa

Figure 14. Interlaminar Shear Stress at the Midplane for $[\pm\theta]_s$ and $[\mp\theta]_s$ Laminates Subjected to a Uniaxial Strain $\bar{\varepsilon}_x = 0.01\%$.

Figures 15 through 17 show the variation of the interlaminar edge stresses as a function of the lay-up angle θ for a $[\pm\theta]_s$ laminate. Two types of loading are considered, mechanical and hygrothermal loadings. The present analysis can handle both types of loadings, including any combination of them. Hygrothermal loading includes a temperature change, a moisture change, or a combination of the two. It can be a constant overall change, or even some distribution of temperature and moisture. However, for simplicity and clarity in the present discussion, the laminate in this example will be loaded separately by a mechanical loading of $\bar{\varepsilon}_x = 0.01$ percent, and a uniform thermal loading of $\Delta T = -50°C$, with the stress free temperature assumed to be room temperature, viz, 21°C. Apart from a small variation due to temperature-dependent material properties, and a sign change, stresses produced by a positive change in temperature are the same as those produced by a negative change.

Several interesting results are noted in comparing the free edge effect of mechanical uniaxial loading and thermal loading, for different values of θ. The interlaminar normal stress σ_z, shown in Figure 15, increases rapidly as θ increases to about 20°, and then decreases; the decrease is much slower beyond $\theta = 45°$. The interlaminar shear stresses (Figures 16 and 17) decrease from zero to a maximum absolute value for values of θ in the range of 20° to 25°. Then they increase again to zero at $\theta = 90°$. Again, beyond $\theta = 45°$, the slope of the curve decreases sharply. The value of θ at which

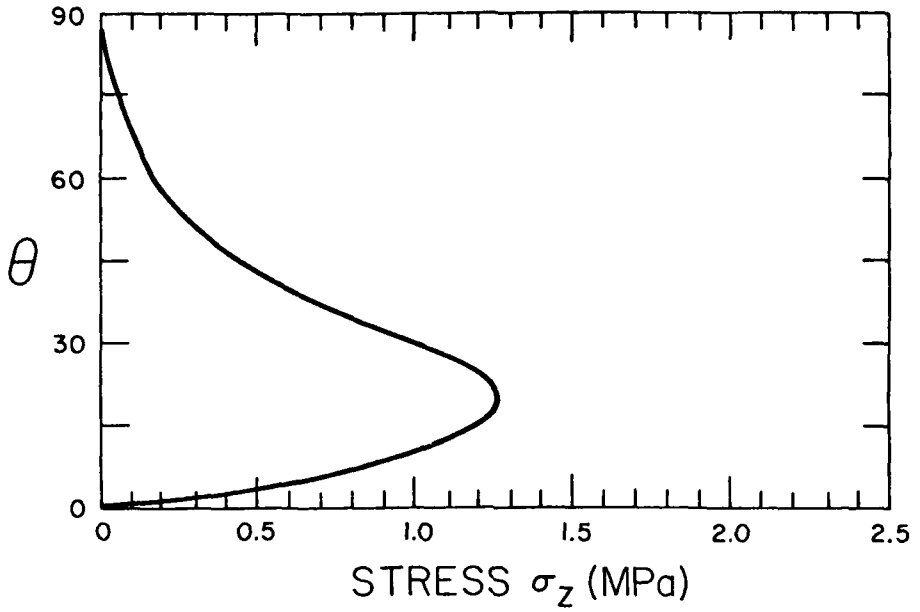

a) Uniaxial Strain $\bar{\varepsilon}_x$ = 0.01%

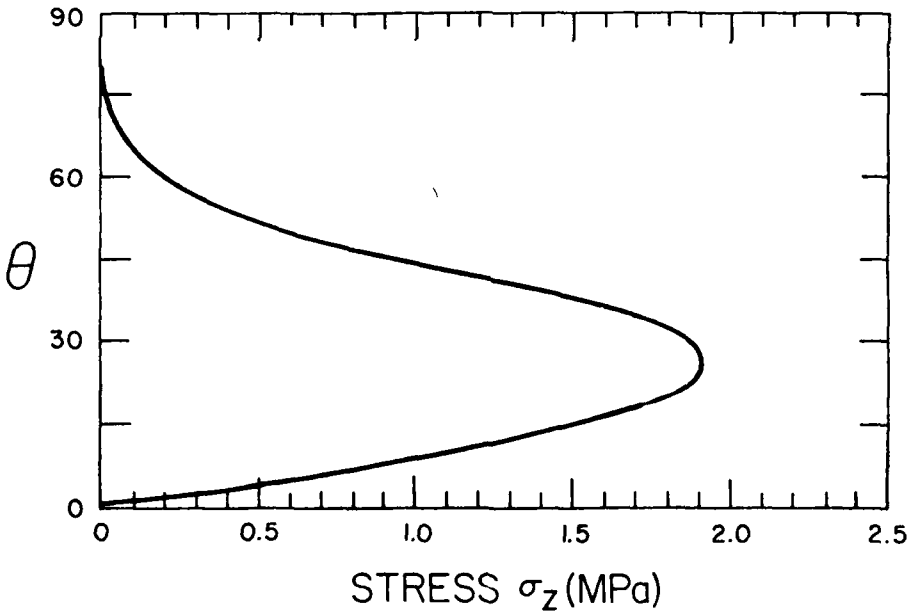

b) ΔT = -50°C

Figure 15. Interlaminar Normal Stress versus Lay-Up Angle for $[\pm\theta]_s$ Laminates.

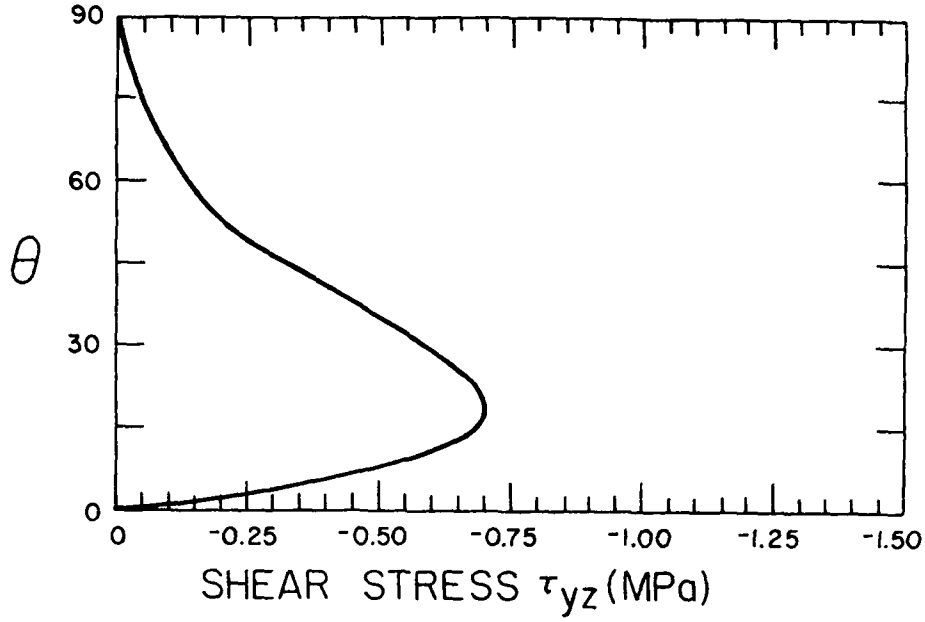

a) Uniaxial Strain $\bar{\varepsilon}_x$ = 0.01%

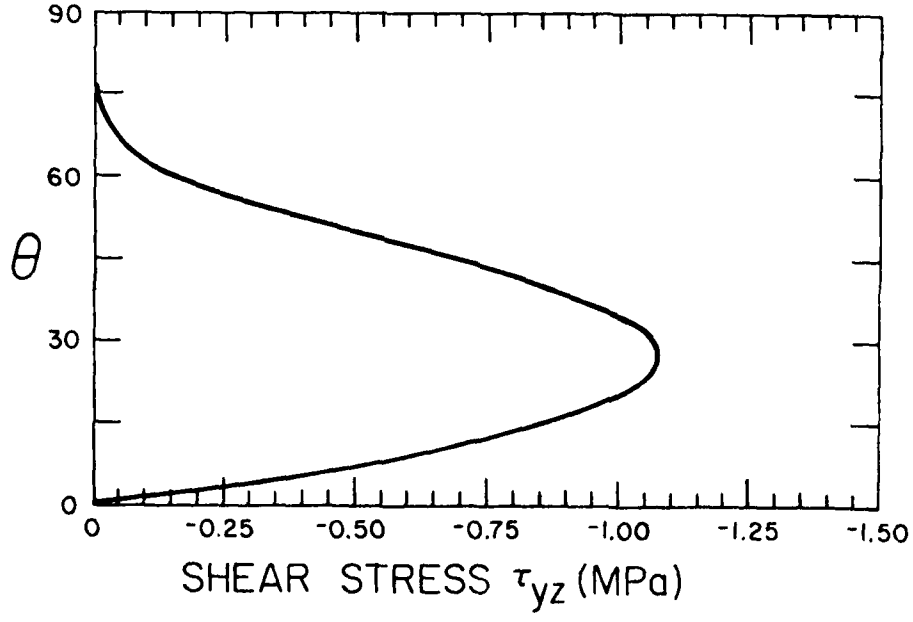

b) ΔT = -50°C

Figure 16. Interlaminar Shear Stress versus Lay-Up Angle for $[\pm\theta]_s$ Laminates.

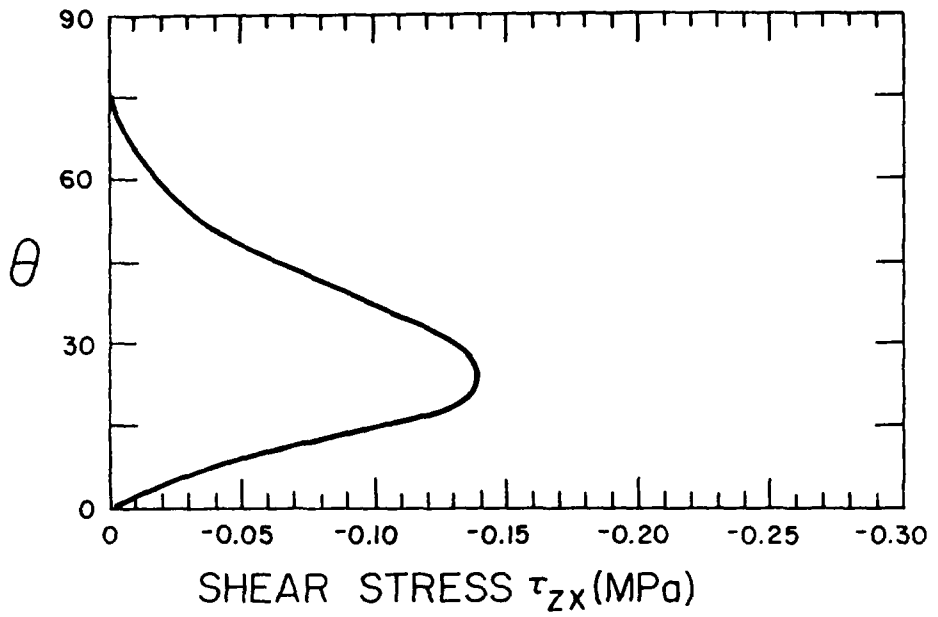

a) Uniaxial Strain $\bar{\varepsilon}_x = 0.01\%$

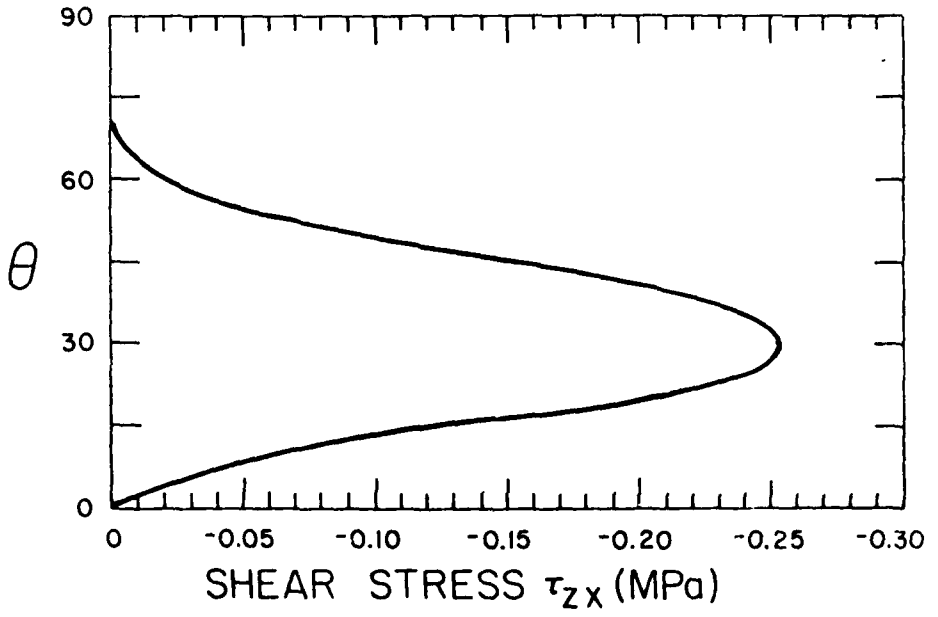

b) $\Delta T = -50°C$

Figure 17. Interlaminar Shear Stress versus Lay-Up Angle for $[\pm\theta]_s$ Laminates.

a peak absolute value is reached by the interlaminar stresses varies under the mechanical loading and thermal loading. Under the thermal loading condition of $\Delta T = -50°C$, this peak value of θ is from 5° to 10° higher than for uniaxial mechanical loading.

Although moisture changes have not been considered in this example, the program is capable of handling hygrothermal loadings due to moisture and/or temperature changes. Moisture changes are handled by the analysis in the same way as temperature changes.

4.4 Interlaminar Stresses Around Circular Holes

The presence of interlaminar stresses near the free edges of laminated plates was demonstrated in the previous two examples. A more complicated and interesting type of problem is that of interlaminar stresses around cutouts, e.g., holes, in laminated composites. Such problems, involving curved rather than straight boundaries, are generally more difficult to analyze. However, since the present analysis is a three-dimensional finite element approach, it is capable of handling any type of boundary geometry with similar ease. The following example illustrates this capability.

The laminates included in this example will be analyzed first under a uniaxial strain ($\bar{\epsilon}_x$ = 0.01 percent) in order to compare results with results using other methods. The multiaxial loading capability will then be demonstrated by applying biaxial loading to the laminates. Finally, inelastic response will be considered. Other methods in the literature cannot handle cases other than

uniaxial loading, since they are based on the uniaxial displacement field first introduced by Pipes and Pagano [26], as discussed earlier. Few earlier analyses considered nonlinear material behavior [20,24]; inelastic laminate response was not considered in any of these methods.

Four-ply laminates of the configurations $[0/90]_s$ and $[90/0]_s$, containing circular holes, are considered. The overall dimensions of the laminate, as given in Reference [43], are:

Length, ℓ = 203 mm

Width, w = 254 mm

Ply thickness, h = 7.6 mm

Hole radius, R = 6.25 mm

The three-dimensional grid used is shown in Figure 18; only one quarter of the upper two layers need be considered, because of symmetry. In the first part of this example, for purposes of comparison, the material assumed is the unidirectional graphite/epoxy composite used in Reference [43], the mechanical properties of which are:

E_{11} = 206 GPa (30 Msi)

$E_{22} = E_{33}$ = 20.7 GPa (3 Msi)

$G_{23} = G_{31} = G_{12}$ = 6.9 GPa (1 Msi)

$\nu_{23} = \nu_{31} = \nu_{12}$ = 0.336

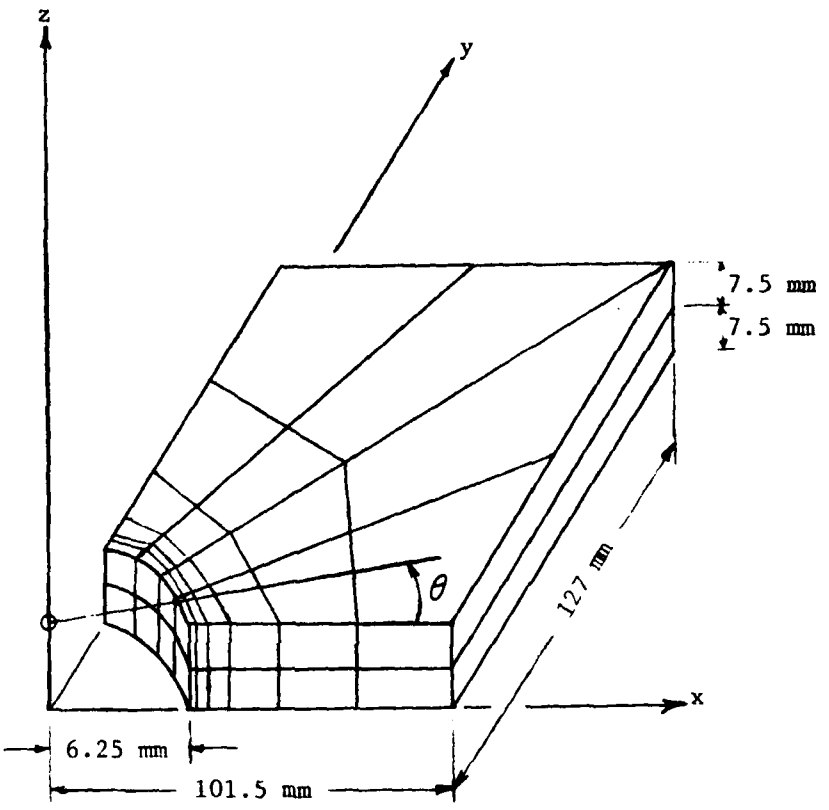

Figure 18. Finite Element Grid Used to Model a Circular Hole in a Four-Ply Laminate.

The distribution of the interlaminar normal stress σ_z is shown in Figure 19 for the two configurations, viz, $[0/90]_s$ and $[90/0]_s$, under a uniaxial strain $\bar{\epsilon}_x$ = 0.01 percent, corresponding to an average applied stress $\bar{\sigma}_x$ = 7.1 MPa. Both laminate configurations show a compressive value for σ_z at $\theta = 0°$, and a tensile value at $\theta = 90°$. Higher values at $\theta = 0°$ and 90° are observed in the $[90/0]_s$

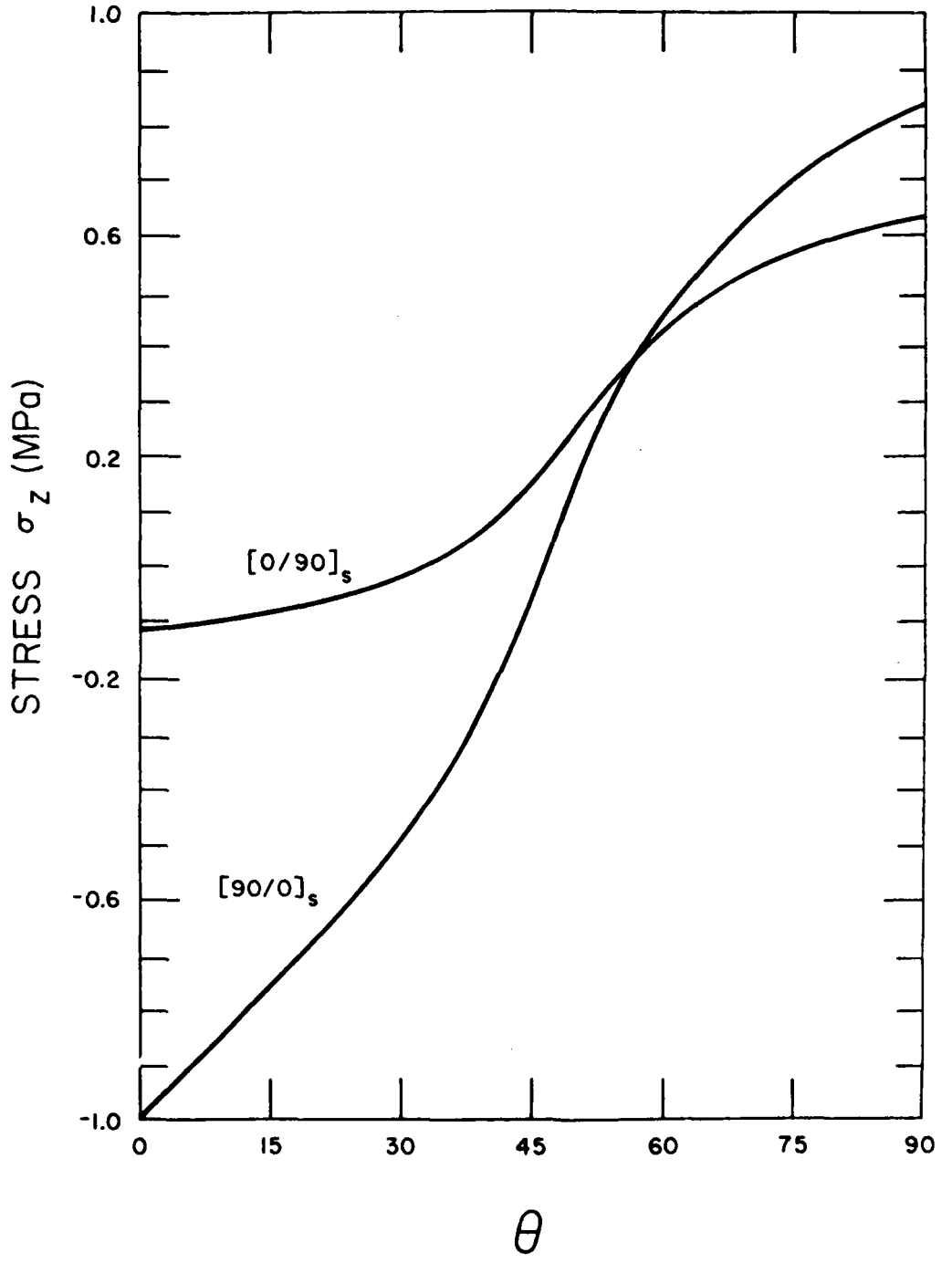

Figure 19. Interlaminar Normal Stress versus Position Around the Free Edge of a Hole in Two Cross-Ply Laminates.

laminate. Thus, the change in stacking sequence does not produce mirror image distributions. Also, in contradiction with results reported in Reference [43], the interlaminar normal stress near the free edge of the hole does not change sign as the stacking sequence is changed.

The analyses of composite laminates under uniaxial loading are helpful in understanding the complex behavior of interlaminar stresses. In actual service, however, laminates are often subjected to multiaxial states of stress. The second part of this example illustrates the capability of the present analysis to handle multiaxial loading situations. Laminates with circular holes, previously analyzed under uniaxial loading, are considered next under varying biaxial loadings.

Table 5 shows the interlaminar normal stress at two different locations, viz, $\theta = 0°$ and $\theta = 90°$, under different biaxial loading conditions. This table has been generated by varying the ratio of $\bar{\varepsilon}_x/\bar{\varepsilon}_y$. For the $[90/0]_s$ laminate, σ_z is always positive at $\theta = 90°$, with almost the same value. This value, shown in column four in Table 5, is reached rapidly from zero under $\bar{\varepsilon}_x/\bar{\varepsilon}_y = 0$ and then attains a constant value at about $\bar{\varepsilon}_x/\bar{\varepsilon}_y = 1$. Plate dimensions and Poisson's ratios appear to affect this behavior; further investigations are needed to fully understand this response. At $\theta = 0°$, σ_z changes from tension to compression as $\bar{\varepsilon}_x$ is increased relative to $\bar{\varepsilon}_y$. For the $[0/90]_s$ configuration, the interlaminar normal stress is always positive at $\theta = 0°$, but the value decreases as the ratio $\bar{\varepsilon}_x/\bar{\varepsilon}_y$ increases. At $\theta = 0°$, σ_z increases from compression to tension as $\bar{\varepsilon}_x/\bar{\varepsilon}_y$ increases.

Predictions such as those given in Table 5 should be very useful to the designer since by estimating the value of $\bar{\varepsilon}_x/\bar{\varepsilon}_y$, a suitable layup can be chosen.

Table 5. Interlaminar Normal Stresses at Two Midplane Locations Around the Free Edge of a Circular Hole in Cross-Ply Laminates.

Ratio of applied strains $\bar{\varepsilon}_x/\bar{\varepsilon}_y$	Interlaminar Normal Stress σ_z (MPa)			
	$[0/90]_s$		$[90/0]_s$	
	θ=0°	θ=90°	θ=0°	θ=90°
0.125	4.0	-3.5	2.0	0.4
0.25	2.0	-2.0	0.7	0.4
0.3	1.7	-1.3	0.5	0.4
0.6	0.6	-0.5	0.03	0.4
1.25	0.4	-0.1	-0.2	0.4
1.5	0.3	-0.03	-0.3	0.4
3	0.15	0.12	-0.4	0.4
5	0.08	0.20	-0.4	0.4
6	0.06	0.20	-0.4	0.4

In spite of the fact that composite materials often exhibit large amounts of inelastic deformation, no method of analysis considered the inelastic behavior of composite laminates. To show hoe the present analysis can handle inelastic material behavior, a different material system is used in the next part of this example. The material is Hercules AS/3501-6 graphite/epoxy, the mechanical properties of which were given in Table 3. The method of analysis of Reference [43] did not consider the inelastic behavior and hence no post elastic properties were presented.

The interlaminar stresses for the two cross-ply configurations were calculated under a biaxial loading ratio $\epsilon_x/\epsilon_y = 1.25$ (see Table 5). Figure 20 is a plot of the interlaminar stresses at the midplane, i.e., at z = 0, while the interlaminar stresses at the interface between the 90° and 0° plies, i.e., at z = h, are shown in Figure 21. For both configurations, the interlaminar normal stress σ_z is dominant at $\theta = 90°$, with a higher tensile value in the $[90/0]_s$ laminate. The variation of σ_z between $\theta = 0°$ and $\theta = 90°$ is much greater at the midplane than at z = h. The interlaminar shear stress τ_{yz} at z = 0 increases in absolute value to a maximum at $\theta = 90°$ for both configurations. However, at z = h, a peak absolute value is attained at $\theta = 45°$. The interlaminar shear stress τ_{zx} behaves in a similar manner at z = h, except for a change in sign, and also attains a peak value at $\theta = 45°$. However, at z = 0, τ_{zx} decreases in absolute value towards a minimum at $\theta = 90°$.

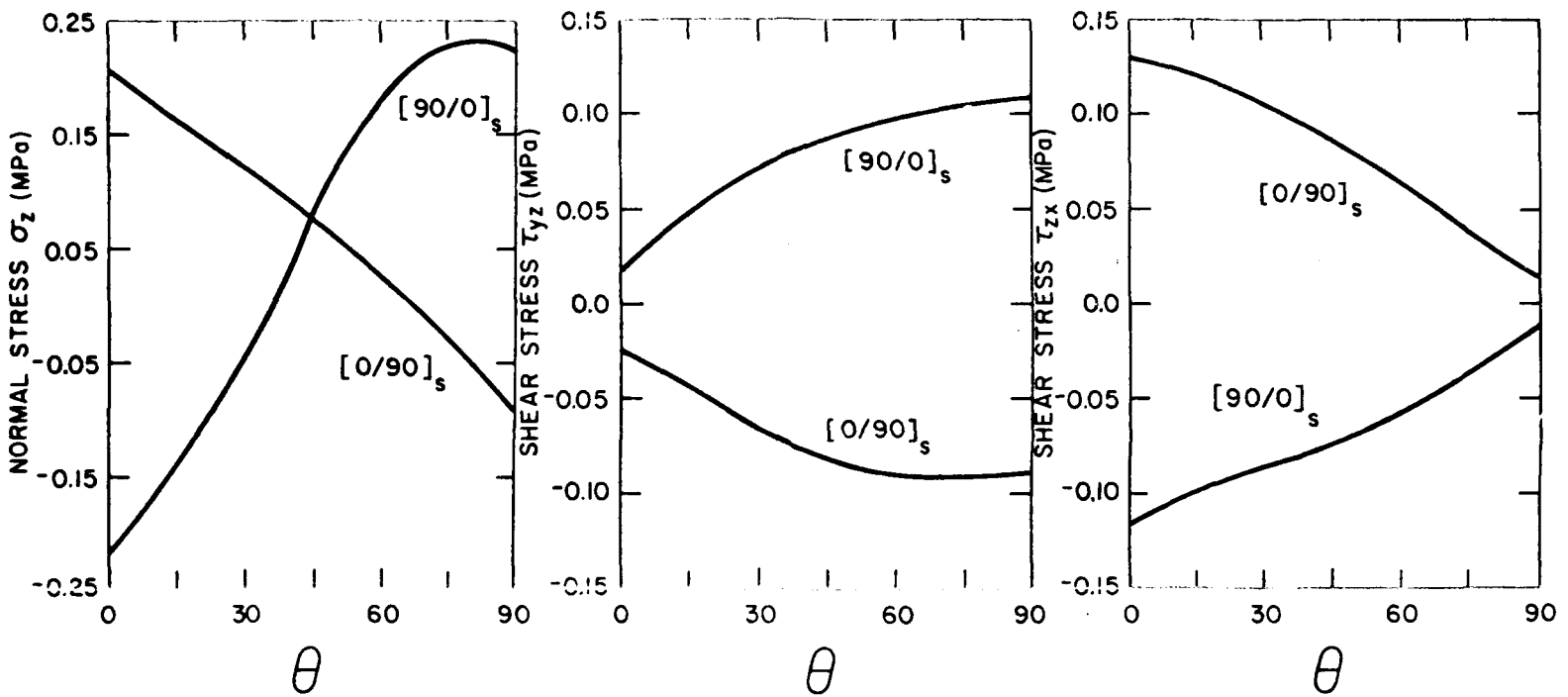

a) Normal Stress σ_z b) Shear Stress τ_{yz} c) Shear Stress τ_{zx}

Figure 20. Interlaminar Stresses Around a Circular Hole at the Midplane, $z = 0$, in $[0/90]_s$ and $[90/0]_s$ Laminates Subjected to Biaxial Loading $\bar{\varepsilon}_x/\bar{\varepsilon}_y = 1.25$.

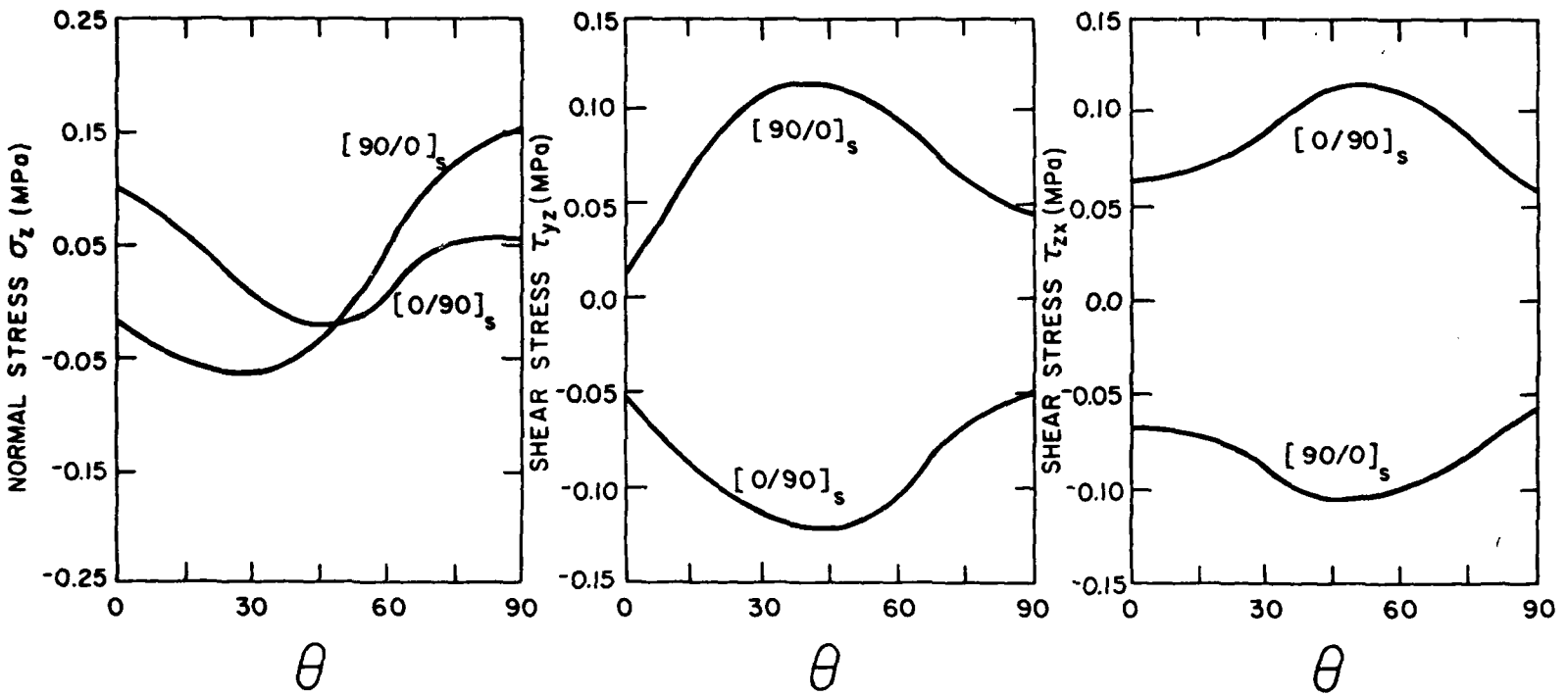

a) Normal Stress σ_z b) Shear Stress τ_{yz} c) Shear Stress τ_{zx}

Figure 21. Interlaminar Stresses Around a Circular Hole at z = h, in $[0/90]_s$ and $[90/0]_s$ Laminates Subjected to Biaxial Loading $\bar{\varepsilon}_x/\bar{\varepsilon}_y = 1.25$.

To study the inelastic behavior of cross-ply laminates, the biaxial loading was increased, keeping the ratio constant. In the case of the $[0/90]_s$ laminate, yielding occured first at the free edge of the hole in the inner 90° ply at an angle slightly less than 45°, and in the outer 0° ply at an angle slightly greater than 45°, as indicated in Figure 22. As the load increased, the yield zone moved across the 45° line in both plies, always beginning in the inner ply, i.e., the 90° ply. Yielding in the $[90/0]_s$ laminate started at the same locations and at the same load level. The progressive growth of the yield zone in each lamina for both configurations is shown in Figure 22. The pattern in which the plastic zone propagated in each ply did not change as the stacking sequence changed. First failure was found to occur at the 45° position, as shown in Figure 23. For both configurations, this first failure was at the free edge of the hole, at the midplane. The state of stress around the free edge of cutouts is indeed very complicated. A method of analysis such as the one presented here is mandatory when designing laminates that will not delaminate at free edges, whether at a straight free edge or around a cutout. The ability of this method to handle hygrothermal loadings makes it of special value in dealing with polymeric composites, which are specially susceptable to changes in temperature and moisture levels. Such changes in environmental conditions often lead to triaxial states of stress, which can only be handled by a full three-dimensional analysis.

AD-A095 147 WYOMING UNIV LARAMIE DEPT OF MECHANICAL ENGINEERING F/G 11/4
THREE-DIMENSIONAL ELASTOPLASTIC FINITE ELEMENT ANALYSIS OF LAMI--ETC(U)
NOV 80 M M MONIB, D F ADAMS, D E WALRATH DAAG29-79-C-0189
UNCLASSIFIED UWME-DR-001-102-1 ARO-16370.4-MS NL

2 OF 2
AD A 095107

END
DATE FILMED
3-81
DTIC

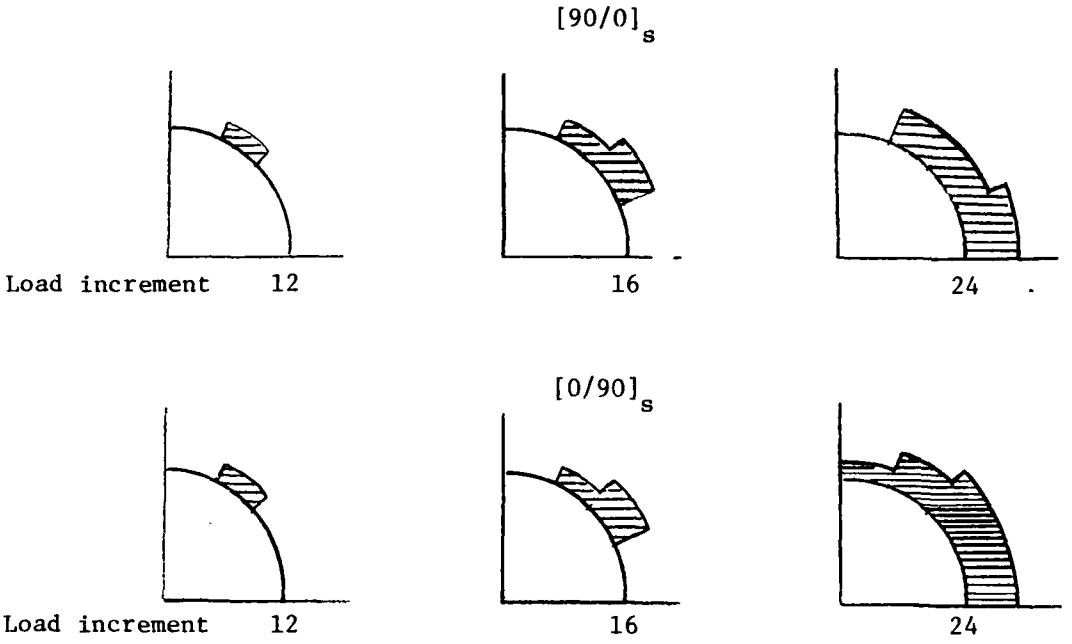

a) Propagation of yield zone in 0° ply

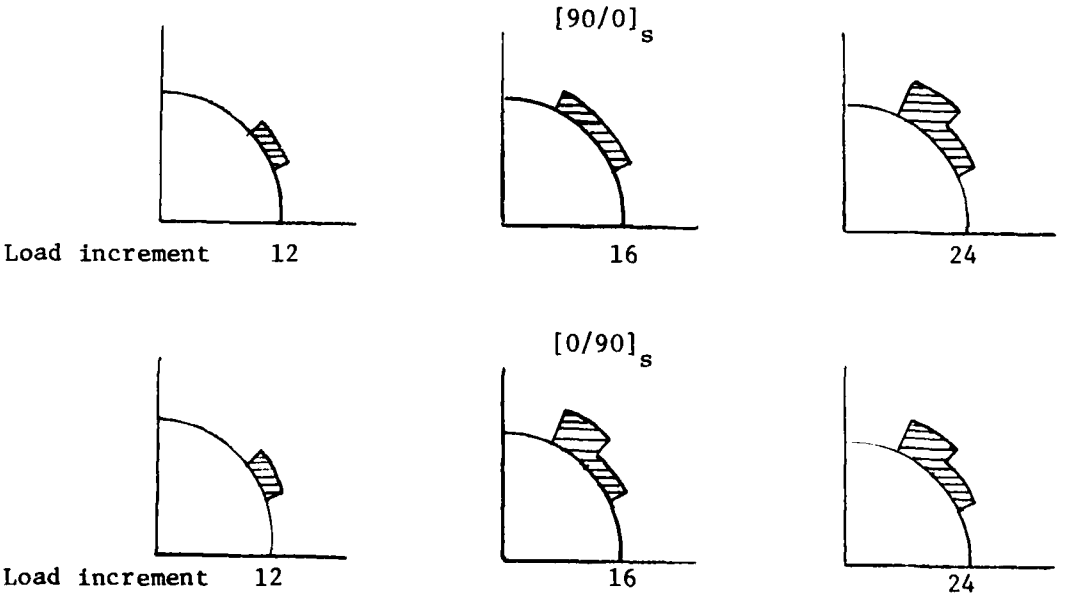

b) Propagation of yield zone in 90° ply

Figure 22. Propagation of Yield Zone under Biaxial Loading $\bar{\epsilon}_x/\bar{\epsilon}_y = 1.25$.

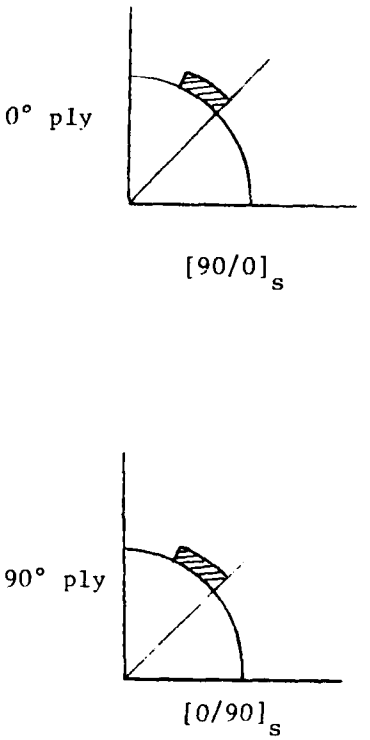

Figure 23. First Failure in Cross-Ply Laminates Under Biaxial Loading.

Section 5

SUMMARY AND CONCLUSIONS

The present study has been concerned with the three-dimensional inelastic problem of generally orthotropic laminated composites, including hygrothermal effects.

At the present time there are not enough experimental data to permit the construction of a 'general' theory of plasticity for composite materials. However, analytical methods such as the one presented here should continue to be investigated and correlated to experimental data, in order to direct future experimental programs toward attaining the goal of a general theory.

The example problems presented in the previous chapter demonstrate only a few of the many potential applications of the analysis. It would be possible to combine several of these features, such as multiaxial loading, mechanical and hygrothermal loading, etc., to model many different situations. The purpose here, however, is to give an indication of the possible uses and applications of the program. Experimental verification of these capabilities remains to be performed.

The analysis is capable of modeling any laminated composite subjected to triaxial mechanical and/or hygrothermal loadings. It can also be used as a three-dimensional micromechanics analysis, since it can model any number of materials simultaneously. Being

a three-dimensional analysis, it is the only way to analyze materials such as 3-D carbon-carbon composites, which consist of yarn bundles oriented in three-dimensions. A three-dimensional finite element analysis is used to model the laminate. The constituent material properties, which can be functions of temperature and moisture content, are input as coefficients of a second order polynomial. This, however, can be changed easily to describe any other functional relationship between the material properties and temperature and moisture. The current version of the computer program uses a finite element analysis based upon a displacement formulation, and linear isoparametric brick elements with three degrees of freedom per node. Other types of elements can be added to the program to model geometrically complex boundaries, crack elements, or any specialized elements such as those of Reference [88]. The modular form in which this program is built makes it a relatively easy task to do so.

Nonlinear (elastoplastic) material behavior is included by means of the tangent modulus method. The onset of plastic deformation is determined by the use of a yield surface which is dependent on both temperature and moisture content in the composite. Work hardening of the material is assumed to be isotropic in the present version of the program, for lack of experimental data to describe this phenomenon otherwise for composite materials. The Bauschinger effect is also neglected for similar reasons. Statistical variations in the properties of typical composite materials, however, may well prove to exceed the small inaccuracies induced by these assumptions.

The failure surface incorporated in the present analysis is similar in shape to the yield surface and is also dependent on temperature and moisture. The failure of any lamina will cause the current computer program to halt execution, with proper messages. This does not always mean that the laminate has failed, however, as discussed earlier. Many composites will continue to carry load long after the matrix has experienced many local failures (microcracks). For this reason, crack propagation should be included in future work. This capability can be incorporated into the present analysis, e.g., by reducing the material stiffness properties of failed elements. Other methods, originally developed for unidirectional composites, such as those discussed in References [89-91] could also be modified to suit the laminate analysis.

The addition of time-dependent deformation into the present analysis is another feasible capability that could be handled. Recently Schaffer and Adams [92] presented a nonlinear viscoelastic analysis for unidirectional composites. In their work, nonlinear viscoelastic constitutive equations for an isotropic material were developed and incorporated in an elastoplastic computer program [18] originally developed for time-independent analyses. To similarly add time-dependent material response to the present work, viscoelastic constitutive equations for a generally orthotropic material will have to be developed.

In summary, the present analysis is a fully three-dimensional, elastoplastic analysis. It can be used to analyze any composite laminate or structure consisting of any number of generally orthotropic materials, for which mechanical properties can vary with both temperature and moisture. Hygrothermal and/or mechanical loadings can be handled.

REFERENCES

1. S. W. Tsai, "Structural Behavior of Composite Materials," NASA CR-71, National Aeronautics and Space Administration, Washginton, D.C., July 1964.

2. E. Reissner and Y. Stavsky, "Bending and Stretching of Certain Types of Heterogeneous Aeolotropic Elastic Plates," J. Appl. Mech., Vol. 28, September 1961, pp. 402-408.

3. C. B. Smith, "Some New Types of Orthotropic Plates Laminated of Orthotropic Material," J. Appl. Mech., Vol. 20, June 1953, pp. 286-288.

4. J. E. Ashton, J. C. Halpin, and P. H. Petit, Primer on Composite Materials: Analysis, Technomic Publishing Co., Stanford, Conn., 1969.

5. J. E. Ashton and J. M. Whitney, Theory of Laminated Plates, Technomic Publishing Co., Stanford, Conn., 1970.

6. H. T. Hahn and N. J. Pagano, "Curing Stresses in Composite Laminates," J. Comp. Mat., Vol. 9, January 1975, pp. 91-106.

7. "Advanced Composites Design Guide, Vol. 2-Analysis," Air Force Materials Laboratory, Dayton, Ohio, 1973.

8. P. H. Petit, "Ultimate Strength of Laminated Composites," General Dynamics/Ft. Worth, FZM 4977, Air Force Contract No. AF33-615-5257, Fort Worth, Texas, 1967.

9. V. D. Azzi and S. W. Tsai, "Elastic Moduli of Laminated Anisotropic Composites," Exp. Mech., Vol. 5, June 1965, pp. 177-185.

10. R. Hill, The Mathematical Theory of Plasticity, Oxford University Press, London, England, 1950.

11. V. D. Azzi and S. W. Tsai, "Anisotropic Strength of Composites," Exp. Mech., Vol. 5, September 1965, pp. 283-288.

12. S. W. Tsai, "Strength Characteristics of Composite Materials," NASA CR-224, National Aeronautics and Space Administration, Washington, D.C., April 1965.

13. K. D. Chiu, "Ultimate Strengths of Laminated Composites," J. Comp. Mat., Vol. 3, July 1969, pp. 578-582.

14. O. Hoffman, "The Brittle Strength of Orthotropic Materials," J. Comp. Mat., Vol. 1, April 1967, pp. 200-207.

15. S. W. Tsai and E. M. Wu, "A General Theory of Strength for Anisotropic Materials," J. Comp. Mat., Vol. 5, January 1971, pp. 58-80.

16. D. F. Adams and D. R. Doner, "Longitudinal Shear Loading of a Unidirectional Composite," J. Comp. Mat., Vol. 1, January 1967, pp. 4-17.

17. R. L. Foye, "Inelastic Micromechanics of Curing Stresses in Composites," Inelastic Behavior of Composite Materials, bound volume of papers presented at the 1975 ASME Winter Annual Meeting, 1975.

18. A. K. Miller and D. F. Adams, "Inelastic Micromechanics Analysis of Graphite/Epoxy Composites Subjected to Hygrothermal Cycling," ASTM Conference: Advanced Composite Materials Environmental Effects, ASTM STP-658, American Society for Testing and Materials, Dayton, Ohio, September 1977.

19. A. K. Miller and D. F. Adams, "Micromechanical Aspects of the Environmental Behavior of Composite Materials," Report UWME-DR-701-1111, Department of Mechanical Engineering, University of Wyoming, Laramie, Wyoming, January 1977.

20. P. H. Petit and M. E. Waddoups, "A Method of Predicting the Nonlinear Behavior of Laminated Composites," J. Comp. Mat., Vol. 3, January 1969, pp. 2-19.

21. Z. Hashin, D. Bagchi, and B. W. Rasen, "Nonlinear Behavior of Fiber Composite Laminates, "NASA CR-NAS1-11284, National Aeronautics and Space Adminsitration, Washington, D.C., September 1973.

22. W. Ramberg and W. B. Osgood, "Description of Stress-Strain Curves by Three Parameters," NASA TN-902, National Advisory Committee for Aeronautics, Washington, D.C., July 1943.

23. R. S. Sandhu, "Ultimate Strength Analysis of Symmetric Laminates," Technical Report AFFDL-TR-73-137, Air Force Flight Dynamics Laboratory, Dayton, Ohio, February 1974.

24. G. D. Renieri and C. T. Herakovich, "Nonlinear Analysis of Laminated Fibrous Composites," Report No. VPI-E-76-10, Virginia Polytechnic Institute, Blacksburg, Virginia, 1976.

25. R. B. Pipes, B. E. Kaminski, and N. J. Pagano, "The Influence of the Free-edge Upon the Strength of Angle-ply Laminates," Test Methods for High Modulus Fibers and Composites, ASTM STP-521, American Society for Testing and Materials, Philadelphia, Pennsylvania, 1972, pp. 218-228.

26. R. B. Pipes and N. J. Pagano, "Interlaminar Stresses in Composite Laminates Under Uniform Axial Extension," J. Comp. Mat., Vol. 4, October 1970, pp. 538-548.

27. R. L. Foye and D. J. Baker, "Design/Analysis Methods for Advanced Composite Structures," Technical Report AFML-TR-70-299, Air Force Materials Laboratory, Dayton, Ohio, February 1971.

28. R. B. Pipes and I. M. Daniel, "Moire Analysis of the Interlaminar Shear Edge Effect in Laminated Composites," J. Comp. Mat., Vol. 5, April 1971, pp. 255-259.

29. R. B. Pipes, "Interlaminar Stresses in Composite Laminates," Technical Report AFML-TR-72-18, Air Force Materials Laboratory, Dayton, Ohio, May 1972.

30. A. H. Puppo and H. A. Evensen, "Interlaminar Shear in Laminated Composites Under Generalized Plane Stress," J. Comp. Mat., Vol. 4, April 1970, pp. 204-220.

31. G. Isakson and A. Levy, "Finite Element Analysis of Interlaminar Shear in Fibrous Composites," J. Comp. Mat., Vol. 5, April 1971, pp. 273-276.

32. A. Levy, H. Armen, Jr., and J. Whiteside, "Elastic and Plastic Interlaminar Shear Deformation in Laminated Composites Under Generalized Plane Stress," Proceedings of the Third Air Force Conference on Matrix Methods in Structural Mechanics, Wright-Patterson Air Force Base, Ohio, October 1971.

33. C. T. Herakovich and E. W. Brooks, Jr., "Tensile Strength Behavior of Composite Reinforced Metals," Report No. VPI-E-73-5, Virginia Polytechnic Institute, Blacksburg, Virginia, January 1973.

34. E. F. Rybicki, "Approximate Three-Dimensional Solutions for Symmetric Laminates Under Inplane Loading," J. Comp. Mat., Vol. 5., July 1971, pp. 354-360.

35. E. Altus, A. Ratem, and M. Shmueli, "Free Edge Effect in Angle Ply Laminates - A New Three Dimensional Finite Difference Solution," J. Comp. Mat., Vol. 14, January 1980, pp. 21-30.

36. N. J. Pagano and R. B. Pipes, "The Influence of Stacking Sequence on Laminate Strength," J. Comp. Mat., Vol. 5, January 1971, pp. 50-57.

37. I. M. Daniel, R. E. Rowlands, and J. B. Whiteside, "Effects of Material and Stacking Sequence on Behavior of Composite Plates with Holes," Exp. Mech., Vol. 14, January 1974, pp. 1-12.

38. N. J. Pagano and R. B. Pipes, "Some Observations on the Interlaminar Strength of Composite Laminates," Int. J. Mech. Sci., Vol. 15, August 1973, pp. 679-688.

39. A. S.D. Wang and F. W. Crossman, "Some New Results on Edge Effects in Symmetric Composite Laminates," J. Comp. Mat., Vol. 11, January 1977, pp. 92-106.

40. J. T.S. Wang and J. N. Dickson, "Interlaminar Stresses in Symmetric Composite Laminates," J. Comp. Mat., Vol. 12, October 1978, pp. 390-402.

41. A. S.D. Wang and F. W. Crossman, "Calculation of Edge Stresses in Multi-Layer Laminates by Sub-Structuring," J. Comp. Mat., Vol. 12, January 1978, pp. 76-83.

42. A. S.D. Wang and F. W. Crossman, "Edge Effects on Thermally Induced Stresses in Composite Laminates," J. Comp. Mat., Vol. 11, July 1977, pp. 300-312.

43. E. F. Rybicki and D. W. Schmueser, "Effect of Stacking Sequence and Lay-up Angle on Free Edge Stresses Around a Hole in a Laminated Plate Under Tension," J. Comp. Mat., Vol. 12, July 1978, pp. 300-313.

44. A. Phillips and R. L. Sierakowski, "On the Concept of the Yield Surface," Acta Mech., Vol. 1, 1965, pp. 29-35.

45. H. Tresca, Comptes Rendus Acad. Sci., Vol. 59, Paris, France, 1864, pp. 754-799.

46. R. von Mises, Gottinger Nachrichten, math.-phys. Klasse, Mathematisch-Physikalische, Nachrichten, 1913, pp. 582-592.

47. J. E. Dorn, "Stress-Strain Relations for Anisotropic Plastic Flow," J. Appl. Phys., Vol. 20, January 1949, pp. 15-20.

48. Y. Yamada, "Recent Developments in Matrix Displacement Method for Elastic-Plastic Problems in Japan, " Advances in Matrix Methods of Structural Analysis and Design, University of Alabama in Huntsville Press, Huntsville, Alabama, 1971, pp. 283-316.

49. L. R. Jackson, K. F. Smith, and W. T. Lankford, "Plastic Flow in Anisotropic Sheet Metal," Metals Tech., T. P. 2440, Vol. 15, May 1948, pp. 1-20.

50. L. W. Hu, "Studies on Plastic Flow of Anisotropic Metals," J. Appl. Mech., Vol. 23, September 1956, pp. 444-450.

51. A. Baltov and A. Sawczuk, "A Rule of Anisotropic Hardening," Acta Mech., Vol. 1, 1965, pp. 81-92.

52. S. W. Tsai, "Strength Theories of Filamentary Structures," Fundamental Aspects of Fiber Reinforced Plastic Composites, Wiley Interscience, New York, New York, 1968, pp. 3-11.

53. F. Narayanaswani and H. M. Adelman, "Evaluation of the Tensor Polynomial and Hoffman Strength Theories for Composite Materials," J. Comp. Mat., Vol. 11, October 1977, pp. 366-377.

54. H. Armen, Jr., "Plastic Analysis," Structural Mechanics Computer Programs, (Edited by W. Pilkey, et al.), University of Virginia Press, Charlottesville, Virginia, 1974, pp. 37-79.

55. P. G. Hodge, Jr., "The Theory of Piecewise Linear Isotropic Plasticity," Proceedings of the IUTAM Colloquium, Madrid, Spain, 1955.

56. W. Prager, "The Theory of Plasticity - A Survey of Recent Achievements," Proc. Inst. Mech. Engrs., Vol. 169, 1955, pp. 41-57.

57. W. Prager, "A New Method of Analyzing Stress and Strain in Work-Hardening Solids," J. Appl. Mech., Vol. 23, December 1956, pp. 493-496.

58. P. G. Hodge, Jr., "A General Theory of Piecewise Linear Plasticity," J. of Appl. Mech. and Phy. of Solids, Vol. , 1957, pp. 242-260.

59. P. Dawez, "On the Plasticity of Crystals," Phys. Rev., Vol. , 1935, pp. 494-501.

60. G. N. White, Jr., "Application of the Theory of Perfectly Plast Solids to Stress Analysis of Strain Hardening Solid ," Tech. Rep. 51, Brown University, Providence, Rhode Island, 1950.

61. J. F. Besseling, "A theory of Plastic Flow for Anisotropic Hardening: Plastic Deformation of an Initially Isotropic Materials," Report 5410, National Aeronautics Research Institute, Amsterdam, Scotland, 1953.

62. Z. Mroz, "On the Description of Anisotropic Work-Hardening," J. Mech. Phys. Solids, Vol. 15, 1967, pp.

63. Z. Mroz, "An Attempt to Describe the Behavior of Metals Under Cyclic Loads Using a More General Work-Harde Acta Mech., Vol. 17, 1969, pp. 199-212.

64. D. C. Drucker, "A More Fundamental Approach to Plastic Stress Strain Relations," Proc. 1st U.S. National Mech., 1952, pp. 487-491.

65. H. Armen, "Assumptions, Models and Computational Methods for Plasticity," Comp. & Struct., Vol. 10, August pp. 161-174.

66. G. N. White, Jr., and D. C. Drucker, "Effective Stress and Effective Strain in Relation to Stress Theories of Plasticity," J. Appl. Phys., Vol. 21, October pp. 1013-1021.

67. M. J. Forray, Variational Calculus in Science and Engineer McGraw-Hill Book Co., New York, New York,

68. R. M. Richard, and J. R. Blacklock, "Finite Element Analysis of Inelastic Structures," AIAA J., Vol. 7, March pp. 432-438.

69. R. M. Richard, and B. J. Abbott, "Versatile Elastic-Plastic Stress-Strain Formula," Proc. ASCE, Vol. 101 (EM4), pp. 511-515.

70. R. D. Cook, Concepts and Applications of Finite Element Analysis, John Wiley and Sons, Inc., New York, New York, 1974.

71. O. C. Zienkiewicz, The Finite Element Method in Engineering Science, McGraw-Hill Book Co., London, 1971.

72. B. M. Irons, "Engineering Application of Numerical Integration in Stiffness Method," AIAA J., Vol. 4, November 1966, pp. 2035-2037.

73. J. G. Eragatoudis, B. M. Irons, and O. C. Zienkiewicz, "Three Dimensional Analysis of Arch Dams and Their Foundations," Proc. of the Symposium on Arch Dams, Institute of Civil Engineering, London, England, 1968.

74. R. W. Clough, "Comparison of Three Dimensional Finite Elements," Proc. of the Symposium on Application of Finite Element Methods in Civil Engineering, Vanderbilt University, Nashville, Tennessee, 1969, pp. 1-26.

75. G. C. Nayak and O. C. Zienkiewicz, "Elasto-Plastic Stress Analysis. Generalization for Various Constitutive Relations Including Strain Softening," Int. J. Num. Meth. Engng., Vol. 5, September 1972, pp. 113-135.

76. R. M. Gallagher, J. Padlog, and P. P. Bijloard, "Stress Analysis of Heated Complex Shapes," J. Aero-Space Sci., 1962, pp. 700-707.

77. J. H. Argyris, "Matrix Analysis of Three Dimensional Media - Small and Large Displacements," J. AIAA, Vol. 3, January 1965, pp. 45-51.

78. R. J. Melosh, "Structural Analysis of Solids," Proc. ASCE, ST-4, August 1963, pp. 205-223.

79. O. C. Zienkiewicz, The Finite Element Method, McGraw-Hill Book Co., London, England, 1967.

80. O. C. Zienkiewicz, B. M. Irons, F. C. Scott, and J. S. Campbell, "Three Dimensional Stress Analysis," Proc. Symposium on High Speed Computing of Elastic Structures, Liege, Belgium, 1970, pp. 413-431.

81. O. C. Zienkiewicz, R. T. Taylor, and J. M. Too, "Reduced Integration Technique in General Analysis of Plates and Shells," Int. J. Num. Meth. Engng., Vol. 3, April 1971, pp. 275-290.

82. B. M. Irons, "A Frontal Solution Technique for Finite Element Analysis," Int. J. Num. Meth. Engng., Vol. 2, January 1970, pp. 5-32.

83. A. Alizadeh and G. T. Will, "A Substructured Frontal Solver and its Application to Localized Material Nonlinearity," Comp. & Struc., Vol. 10, September 1979, pp. 225-231.

84. D. K.Y. Kan, "A Simple Front Solution Technique for Finite Element Method," Report CNME-CR-51, Dept. of Civil Engineering, University College of Swansea, Swansea, U.K., 1971.

85. D. F. Adams and A. K. Miller, "The Influence of Transverse Shear on the Static Flexure and Charpy Impact Response of Hybrid Composite Materials," J. Mat. Sci., Vol. 11, 1976, pp. 1697-1710.

86. D. F. Adams and A. K. Miller, "An Analysis of the Impact Behavior of Hybrid Composite Materials," Mat. Sci. Eng., Vol. 19, 1975, pp. 245-260.

87. *Unpublished Experimental Data for Hercules* AS/3501-6 Graphite/ Epoxy Unidirectional Composite Material, Department of Mechanical Engineering, University of Wyoming, Laramie, Wyoming, 1978.

88. R. L. Spilker, and S. C. Chou, "Edge Effects in Symmetric Composite Laminates: Importance of Satisfying the Traction-Free-Edge Condition," J. Comp. Mat., Vol. 14, January 1980, pp. 2-20.

89. D. F. Adams, "High-Performance Composite Materials for Vehicle Construction: An Elastoplastic Analysis of Crack Propagation in a Unidirectional Composite," Report R-1070-PR, The Rand Corporation, Santa Monica, California, March 1973.

90. D. F. Adams, "Elastoplastic Crack Propagation in Transversely Loaded Unidirectional Composite," J. Comp. Mat., Vol. 8, January 1974, pp. 38-54.

91. D. P. Murphy and D. F. Adams, "Energy Absorption Mechanisms During Crack Propagation in Metal Matrix Composites," Report UWME-DR-901-103-1, Department of Mechanical Engineering, University of Wyoming, Laramie, Wyoming, October 1979.

92. B. G. Schaffer, and D. F. Adams, "Nonlinear Viscoelastic Behavior of a Composite Material Using a Finite Element Micromechanics Analysis," Report UWME-DR-001-101-1, Department of Mechanical Engineering, University of Wyoming, Laramie, Wyoming, June 1980.

APPENDIX A

TRANSFORMATION EQUATIONS FOR STRESS COMPONENTS FOR A FIBROUS LAMINA

Assume that the stress components of a certain lamina are known in the reference axes (x,y,z), and that the axes of anisotropy for this lamina are (1,2,3) such that the 3-axis and z-axis coincide. Then, if the 1-axis is inclined at a counterclockwise angle θ to the x-axis, the stress components in the (1,2,3) system can be found according to the equations

$$\sigma_1 = \sigma_x \cos^2 \theta + \sigma_y \sin^2 \theta + 2\tau_{xy} \sin \theta \cos \theta$$

$$\sigma_2 = \sigma_x \sin^2 \theta + \sigma_y \cos^2 \theta - 2\tau_{xy} \sin \theta \cos \theta$$

$$\sigma_3 = \sigma_z$$

$$\tau_{23} = \tau_{yz} \cos \theta - \tau_{zx} \sin \theta$$

$$\tau_{31} = \tau_{yz} \sin \theta + \tau_{zx} \cos \theta$$

$$\tau_{12} = (\sigma_y - \sigma_x)\sin \theta \cos \theta + \tau_{xy}(\cos^2 \theta - \sin^2 \theta)$$

APPENDIX B

FORMULATION OF STIFFNESS MATRIX FOR AN ISOPARAMETRIC ELEMENT

Consider the local coordinates ξ, η, and ζ, with the origin located at the center of the element as shown in Figure B1. These coordinates will be so defined as to give values of +1 and -1 on the faces of the element. Thus, in this coordinate system the element is a cube, Figure B2. In general, the coordinates of any point are defined by the expressions

$$x = N_1x_1 + N_2x_2 + \ldots + N_8x_8 = \sum_1^8 N_ix_i$$

$$y = \sum_1^8 N_iy_i \qquad \text{(B-1)}$$

$$z = \sum_1^8 N_iz_i$$

where x_i, y_i, and z_i are the nodal coordinates in (x,y,z) system and N_i are the shape functions. Displacements are defined in the same way; hence the name isoparametric.

$$u = \sum_1^8 N_iu_i$$

$$v = \sum_1^8 N_iv_i \qquad \text{(B-2)}$$

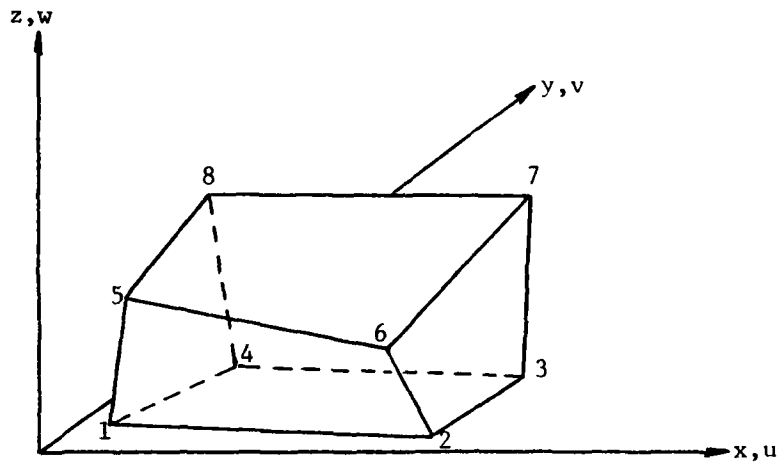

Figure B1. Element in (x,y,z) System of Coordinates.

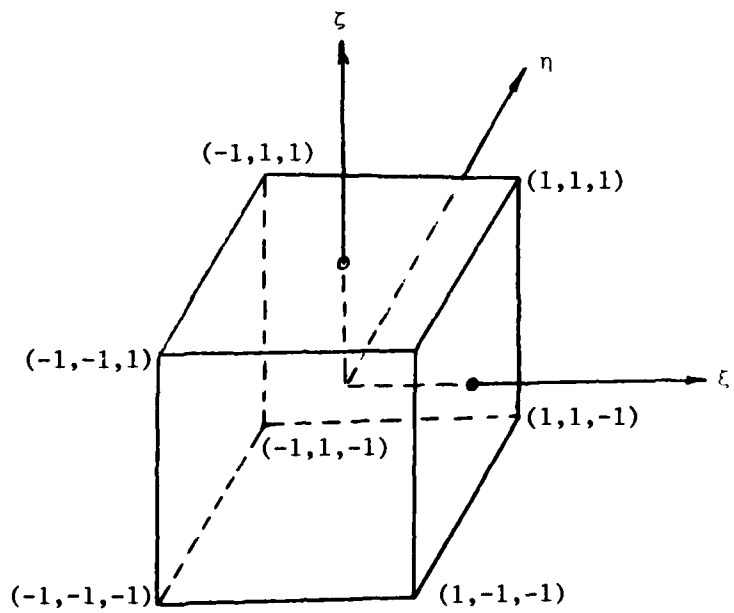

Figure B2. Element in Local (ξ,η,ζ) System of Coordinates.

$$w = \sum_{1}^{8} N_i w_i$$

where u_i, v_i, and w_i are nodal displacements in the x, y, and z directions, respectively, and i ranges from 1 to the total number of nodes (8 in this example of an eight-node quadrilateral element).

The shape functions N_i are given by

$$N_i = \frac{1}{8}(1 + \xi\xi_i)(1 + \eta\eta_i)(1 + \zeta\zeta_i) \tag{B-3}$$

where ξ_i, η_i, and ζ_i are the nodal values, i.e., ± 1.

The element matrices are formulated next, in terms of the isoparametric coordinates. Relations between derivatives in the two coordinate systems are established by the chain rule of differentiation,

$$\begin{Bmatrix} (\ ),_\xi \\ (\ ),_\eta \\ (\ ),_\zeta \end{Bmatrix} = \begin{bmatrix} x,_\xi & y,_\xi & z,_\xi \\ x,_\eta & y,_\eta & z,_\eta \\ x,_\zeta & y,_\zeta & z,_\zeta \end{bmatrix} \begin{Bmatrix} (\ ),_x \\ (\ ),_y \\ (\ ),_z \end{Bmatrix} = [J] \begin{Bmatrix} (\ ),_x \\ (\ ),_y \\ (\ ),_z \end{Bmatrix} \tag{B-4}$$

where commas denote partial differentiation, and [J] is the so-called Jacobian matrix. From Eq. (B-1),

$$[J] = \begin{bmatrix} \partial N_1/\partial\xi & \cdots\cdots & \partial N_8/\partial\xi \\ \partial N_1/\partial\eta & & \partial N_8/\partial\eta \\ \partial N_1/\partial\zeta & & \partial N_8/\partial\zeta \end{bmatrix} \begin{bmatrix} x_1 & y_1 & z_1 \\ x_2 & y_2 & z_2 \\ x_3 & \vdots & \vdots \\ x_4 & \vdots & \vdots \\ x_5 & \vdots & \vdots \\ \vdots & \vdots & \vdots \\ x_8 & y_8 & z_8 \end{bmatrix} \tag{B-5}$$

Using the inverse of Eq. (B-4) on Eq. (B-2)

$$\begin{Bmatrix} u,_x \\ u,_y \\ u,_z \\ v,_x \\ v,_y \\ v,_z \\ w,_x \\ w,_y \\ w,_z \end{Bmatrix} = \begin{bmatrix} A & 0 & 0 \\ 0 & A & 0 \\ 0 & 0 & A \end{bmatrix} \begin{Bmatrix} u,_\xi \\ u,_\eta \\ \cdot \\ \cdot \\ \cdot \\ \cdot \\ \cdot \\ \cdot \\ w,_\zeta \end{Bmatrix} \tag{B-6}$$

where

$$[A] = \begin{bmatrix} a_{11} & a_{12} & a_{13} \\ a_{21} & a_{22} & a_{23} \\ a_{31} & a_{32} & a_{33} \end{bmatrix}$$

and $a_{11} = J_{11}^{-1}$, etc.

But the strain-displacement relation can be written as

$$\{\varepsilon\} = \begin{Bmatrix} \varepsilon_x \\ \varepsilon_y \\ \varepsilon_z \\ \gamma_{yz} \\ \gamma_{zx} \\ \gamma_{xy} \end{Bmatrix} = \begin{bmatrix} 1 & 0 & 0 & 0 & 0 & 0 & 0 & 0 & 0 \\ 0 & 0 & 0 & 0 & 1 & 0 & 0 & 0 & 0 \\ 0 & 0 & 0 & 0 & 0 & 0 & 0 & 0 & 1 \\ 0 & 0 & 0 & 0 & 0 & 1 & 0 & 1 & 0 \\ 0 & 0 & 1 & 0 & 0 & 0 & 1 & 0 & 0 \\ 0 & 1 & 0 & 1 & 0 & 0 & 0 & 0 & 0 \end{bmatrix} \begin{Bmatrix} u_{,x} \\ u_{,y} \\ u_{,z} \\ v_{,x} \\ v_{,y} \\ v_{,z} \\ w_{,x} \\ w_{,y} \\ w_{,z} \end{Bmatrix} \tag{B-7}$$

Substituting from Eq. (B-6) into Eq. (B-7), and utilizing Eq. (B-2), the relation between the strain and displacement is obtained

$$\{\varepsilon\} = [B]\{d\} \tag{B-8}$$

where

$$\{d\} = \begin{Bmatrix} u_1 \\ v_1 \\ u_2 \\ v_2 \\ w_2 \\ \vdots \\ w_8 \end{Bmatrix} \tag{B-9}$$

is the displacement vector.

The element stiffness matrix is then formed as

$$[k] = \int_{Vol.} [B^T][\bar{C}][B]d(Vol.) \qquad (B\text{-}10)$$

where $[\bar{C}]$ is the element stiffness matrix as given in Appendix C.

APPENDIX C

GENERALLY ORTHOTROPIC STIFFNESS COEFFICIENTS

The $\bar{C}$ coefficients in the generally orthotropic stiffness matrix in Eq.(B-10) are listed below:

$$\bar{C}_{11} = U_1 + U_2 \cos(2\theta) + U_3 \cos(4\theta)$$

$$\bar{C}_{12} = U_4 + U_3 \cos(4\theta)$$

$$\bar{C}_{13} = \cos^2\theta\, C_{13} + \sin^2\theta\, C_{23}$$

$$\bar{C}_{14} = \bar{C}_{15} = 0$$

$$\bar{C}_{16} = \tfrac{1}{2} U_2 \sin(2\theta) - U_3 \sin(4\theta)$$

$$\bar{C}_{22} = U_1 - U_2 \cos(2\theta) + U_3 \cos(4\theta)$$

$$\bar{C}_{23} = \sin^2\theta\, C_{13} + \cos^2\theta\, C_{23}$$

$$\bar{C}_{24} = \bar{C}_{25} = 0$$

$$\bar{C}_{26} = -\tfrac{1}{2} U_2 \sin 2\theta + U_3 \sin(4\theta)$$

$$\bar{C}_{33} = C_{33}$$

$$\bar{C}_{34} = \bar{C}_{35} = 0$$

$$\bar{C}_{36} = \sin\theta \cos\theta\, C_{13} - \sin\theta \cos\theta\, C_{23}$$

$$\bar{C}_{44} = \cos^2\theta\, C_{44} + \sin^2\theta\, C_{55}$$

$$\bar{C}_{45} = \sin\theta \cos\theta\, C_{44} + \sin\theta \cos\theta\, C_{55}$$

$$\bar{C}_{46} = 0$$

$$\bar{C}_{55} = \sin^2\theta\, C_{44} + \cos^2\theta\, C_{55}$$

$$\bar{C}_{56} = 0$$

$$\bar{C}_{66} = U_5 - U_3 \cos(4\theta)$$

where

$$U_1 = 1/8\ (3C_{11} + 3C_{12} + 4C_{66})$$

$$U_2 = \tfrac{1}{2}\ (C_{11} - C_{22})$$

$$U_3 = 1/8\ (C_{11} + C_{22} - 2C_{12} - 4C_{66})$$

$$U_5 = 1/8\ (C_{11} + C_{22} - 2C_{12} + 4C_{66})$$

$$C_{11} = (1 - \nu_{23}\ \nu_{22})\ VE_{11}$$

$$C_{22} = (1 - \nu_{31}\ \nu_{13})\ VE_{22}$$

$$C_{33} = (1 - \nu_{12}\ \nu_{21})\ VE_{33}$$

$$C_{12} = (\nu_{21} + \nu_{23}\ \nu_{31})\ VE_{11} = (\nu_{12} + \nu_{13}\ \nu_{32})\ VE_{22}$$

$$C_{13} = (\nu_{31} + \nu_{21}\ \nu_{32})\ VE_{11} = (\nu_{13} + \nu_{23}\ \nu_{12})\ VE_{33}$$

$$C_{23} = (\nu_{32} + \nu_{12}\ \nu_{31})\ VE_{22} = (\nu_{23} + \nu_{21}\ \nu_{13})\ VE_{33}$$

$$C_{44} = G_{23}$$

$$C_{55} = G_{31}$$

$$C_{66} = G_{12}$$

$$V = (1 - \nu_{12}\ \nu_{21} - \nu_{23}\ \nu_{32} - \nu_{13}\ \nu_{31} - \nu_{12}\ \nu_{23}\ \nu_{31})^{-1}$$

APPENDIX D

INPUT INSTRUCTIONS FOR NCLAP

Card 1 (80A1)

TITLE	Problem title

Card 2 (11I5)

NTP	Total number of nodes	
NTE	Total number of elements	
NPE	Number of nodes per element	
NMAT	Number of materials	
NLI	Number of load increments	
NFIX	Number of constrained nodes	
NGAUS	Number of integration points	
ICHK	= 1	Check input data
	= 0	No check
ISTR	= 0	Print element average stresses
	= 1	Print element stresses at every Gaus point
	= 2	Full print out of stresses
IDIS	= 0	No print out of displacements
	= 1	Print accumulated displacements
	= 2	Print incremental and accumulated displacements

IHYG	= 1	Print nodal temperatures and moisture distribution
	= 0	No hygrothermal information printed

Cards 3 (10I5,F10.0,I5)

NE		Element number
NOE		Vector of element connectivity
IMAT		Element material number
ANGLE		Element material angle, i.e., angle between principal direction 1 of the material and the x-axis measured clockwise
IFLOD	= 1	Mechanical load applied to element
	= 0	No mechanical load applied

Cards 4 (I5,5F10.0)

NP	Node number
COORD	Nodal coordinates (x,y,z)
STEMP	Nodal temperature
SMOIS	Nodal moisture content

Cards 5 (I5,2X,3I1,3F10.0)

NFIXP		Constrained node number
CODE		Vector of constraining code
	= 1	Contrained displacement
	= 0	No constraint
CDIS		Prescribed displacements in x, y, and z directions

Card 6 (I5)

MAT	Material number

Cards 7 (6E10.4)

PROPS	Material properties (see Tables 3,4)

Card 8 (2I2)

IMLD	Mechanical loading flag	
	= 1	Increment contains applied mechanical load
	= 0	No mechanical load
IHGR	= 0	No hygrothermal load
	= 1	Uniform change in hygrothermal loading
	= -1	Hygrothermal distribution

Cards 9 (2F10.0)

DTEMP	Uniform applied temperature change
DMOIS	Uniform applied moisture change

Card 10 (2I5)

NE	Mechanically loaded element number
LNODS	Number of nodes loaded

Cards 11 (I5,3F10.0)

LN	Loaded node number
XL,YL,ZL	x-load, y-load, and z-load

Note If IHGR on Card 8 is equal to -1,Cards 9 would then give the change of temperature and moisture for all nodal points ending with the last node. Cards 9 are omitted totally if IHGR is zero.

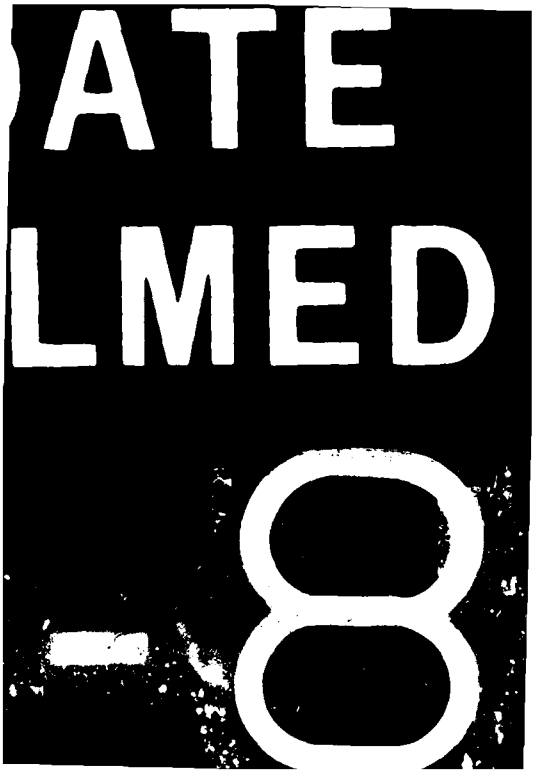
ATE
LMED
8